Fuel 358 (2024) 130160

Contents lists available at ScienceDirect

Fuel

journal homepage: www.elsevier.com/locate/fuel

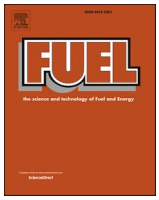

Full Length Article

Multi-criteria optimization of a new geothermal driven integrated power and hydrogen production system via a new Index: Economic sustainability (EcoSI)

Oguz Arslan [a,*], Asli Ergenekon Arslan [b]

[a] Mechanical Engineering Department, Engineering Faculty, Bilecik Seyh Edebali University, Bilecik, 11230, Turkey
[b] Quality Control in Manufacturing, Vocational School, Bilecik Seyh Edebali University, Bilecik, 11230, Turkey

ARTICLE INFO

Keywords:
Economic sustainability index (EcoSI)
Efficiency analysis technique with output satisficing (EATWOS)
Geothermal
Organic Rankine cycle (ORC)
Proton exchange membrane electrolyzer (PEMEL)

ABSTRACT

This study investigates a new geothermal energy-driven hybrid system, including an organic Rankine cycle (ORC) for power generation and a proton exchange membrane electrolyzer (PEMEL) to improve the sustainability of issued geothermal energy sources. In this aim, 2400 designs were formed parametrically. The designs were optimized throughout the multi-criteria decision-making (MCDM) analysis named efficiency analysis technique with output satisficing (EATWOS). In the optimization, a new index named the economic sustainability index (EcoSI) was proposed as the objective function. EcoSI was then introduced into MCDM analysis along with the sustainability index (SI). Design 1–2-7–1-1 with a turbine inlet temperature of 100 °C and inlet pressure of 1950 kPa was determined as the optimal design. In this design, the optimal current density was determined as the minimum chosen value with 1000 A/m^2. The power supply rate was determined as the minimum chosen value of 10 %. The temperatures of the production and re-injection wells were determined as 133.5 °C and 111.99 °C, respectively. The exergy efficiency and power generation rate of ORC were determined as 21.11 % and 12.113 MW, respectively. The hydrogen generation rate and exergy efficiency of PEMEL were determined as 0.0057003 kg/s and 48.76 %, respectively. The exergy efficiency of the overall system was determined as 19.92 %. The investment cost was determined as 332.57 $/h. Exergy destruction, fuel and product costs were determined at 38312.99 $/h, 48272.40 $/h, and 24240.05 $/h, respectively. The sustainability index (SI) was determined as 1.249, whereas the economic sustainability index (EcoSI) was determined as 1.260.

1. Introduction

Geothermal resources are stable energy sources since they are independent of weather conditions. This stability makes geothermal sources preferable in energy systems. Although geothermal energy is a renewable energy source, resources are finite due to the reservoir capacity. So, geothermal energy systems should be designed sensitively to expand sustainability.

Geothermal resources are commonly used for power generation throughout the organic Rankine cycle (ORC) systems with lower efficiency [1,2]. Chitgar et al. [3] reported that it is available to generate power with an exergy efficiency ranging between 37.02 % and 45.06 % from geothermal resources. Altun and Kilic [4] reported that it is available to generate power with an energy efficiency of 11.24 % and exergy efficiency of 39.03 % from geothermal resources at 121 °C. Ozcan and Ekici [5] reported that it is available to generate power with an energy efficiency ranging between 2.19 %and 5.32 %, and exergy efficiency between 11.69 % and 28.41 % from geothermal resources with 172.94 °C. Liu et al. [6] reported that it is available to generate power with an energy efficiency of approximately 7 % and an exergy efficiency of approximately 10 % from geothermal resources at 80 °C. In recent years, integrated systems have drawn attention to increasing resource sustainability since sustainability is directly relevant to system efficiency. The integrated systems include power generation along with heating [7,8], cooling [9–11], and desalination [12,13]. In recent years, hydrogen production has become prominent since hydrogen was handled as an environmentally friendly alternative energy source and storage technique. In hydrogen production, renewable energy sources such as geothermal energy are commonly integrated into hydrogen generation systems [14]. Karayel et al. [15] indicated that it is possible to evaluate the low-temperature geothermal resources for hydrogen

* Corresponding author.
E-mail address: oguz.arslan@bilecik.edu.tr (O. Arslan).

https://doi.org/10.1016/j.fuel.2023.130160
Received 3 September 2023; Received in revised form 18 October 2023; Accepted 22 October 2023
Available online 31 October 2023

Nomenclature

A	Area (m^2)
c	Unit cost of exergy flow ($/MJ)
$\dot{C}$	Exergy cost rate ($/h)
C_p	Specific heat (kJ/kgK)
d	Diameter (m)
E	Multi-criteria efficiency
$EcoSI$	Economic sustainability index
$\dot{E}$	Energy rate (kW)
$\dot{E}x$	Exergy rate (kW)
F	Correction factor
h	Convective heat transfer coefficient (W/m^2K) or Enthalpy (kJ/kg)
ip	Distance matrices for input (kg/m^2s)
J	Dimensionless heat factor or Current density (A/m^2)
k	Conductive heat transfer coefficient (W/mK)
$\dot{m}$	Mass flow rate (kg/s)
MAPE	Mean absolute percentage error (%)
Nu	Nusselt number
op	Distance matrices for output
P	Pressure (kPa, bar or atm)
Pr	Prandtl number
$\dot{Q}$	Heat rate (kW)
r	Normalized output
R^2	Determination coefficient
Re	Reynolds number
s	Specific entropy (kW/kgK) or normalized input
SI	Sustainability index
T	Temperature (K or ^oC)
U	Total heat transfer coefficient (W/m^2K)
v	Weight for output
V	Volume (m^3)
w	Weight for input
$\dot{W}$	Work rate (kW)
x	Input value, mole fraction
y	Output value
$\dot{Z}$	Investment cost

Greek symbols

ε	Exergy efficiency (%)
η	Energy efficiency (%)
f	Friction factor
ν	Specific volume (m^3/kg)
ρ	Density (kg/m^3)
ψ	Specific flow exergy (kJ/kg)
Γ	Mass velocity

Subscripts

a	Anode
act	Activation
c	Cathode
d	Destruction
e	Enforced convective, Electricity saving
F	Fuel
g	Gas phase
h	Hydraulic
i	Inner, inlet, or i^{th} component
lm	Logarithmic mean
o	Outer, outlet
ohm	Ohmic
P	Product
T	Value at a specified temperature
0	Value at the reference state

Abbreviations

C	Compressor
Con	Condenser
Eva	Evaporator
HE	Heat exchanger
HST	Hydrogen storage tank
MCDM	Multi-criteria decision making
ORC	Organic Rankine cycle
P	Pump
PEMEL	Proton exchange membrane electrolyzer
PW	Production well
RW	Re-injection well
T/G	Turbine/Generator group
S	Separator

generation through the Alkaline and proton exchange membrane electrolyzer (PEMEL), whereas the high-temperature geothermal resources can be evaluated in solid oxide electrolyzer. Many studies about geothermal-driven hydrogen generation systems were conducted. Cao et al. [16] investigated the geothermal-driven hydrogen generation. They proposed a hybrid system, including a two-stage ORC and a PEMEL system. They reported that it was possible to achieve an energy efficiency between 11.8 % and 14.8 % and an exergy efficiency between 24.1 % and 28.2 % from the geothermal resource at 200 °C. Ghaebi et al. [17] investigated geothermal energy-driven ORC-integrated PEMEL for power and hydrogen generation. They reported that it is possible to achieve an energy efficiency ranging between 3.32 % and 3.51 % and an exergy efficiency ranging between 64.86 % and 67.58 % from the geothermal resource with 96 °C. Yilmaz [18] investigated a geothermal energy-driven ORC-PEMEL hybrid system. He reported that it is available to achieve an energy efficiency of 6.5 % and an exergy efficiency of 32.4 %. The generated hydrogen was calculated as 0.05 kg/s in the study. Yilmaz [19], in another study, investigated a geothermal energy-driven Flash-ORC-PEMEL hybrid system. He reported that it is available to achieve an energy efficiency of 8.489 % and an exergy efficiency of 38.44 %. The generated hydrogen was calculated as 0.05269 kg/s in the study. Mofrad et al. [20] investigated the geothermal-driven cogeneration system, including dual-pressure ORC and PEMEL. Zeotropic mixture was used as the working fluid in ORC. They reported an energy efficiency of 19.34 % and an exergy efficiency of 58.67 %. Baltacıoglu et al. [21] investigated the hydrogen generation by geothermal energy. ORC was used for electricity generation to drive a PEMEL electrolyzer. A hydrogen generation of more than 4000 kg/day was reported. PEMEL efficiency was found to be within 62–64 %. Kianfard et al. [22] investigated hydrogen generation via PEMEL and desalination, in which a dual-fluid ORC supplied the required power. It was reported that the PEMEL increases the efficiency of the overall system. The overall exergy efficiency was 17.56 %, whereas the single ORC was 47.77 %. Yuksel et al. [23] investigated the hydrogen generation via PEMEL. The required power of PEMEL was supplied from the geothermal energy-driven Kalina cycle (KC). The exergetic efficiency of the single PEMEL was reported as 52.27 %, whereas the overall system's exergy efficiency was 52.63 %. Ratlamwala and Dincer [24] investigated geothermal-driven power generation via flash cycle and hydrogen generation via PEMEL. It was concluded that it is possible to achieve exergy efficiency from 6.52 % to 47.29 %, depending on the flash stages. Yuksel et al. [25] investigated the design variables of hydrogen generation via PEMEL. The required power was supplied from KC driven by geothermal energy. Exergetic efficiency from 32 % to 58 % was reported depending

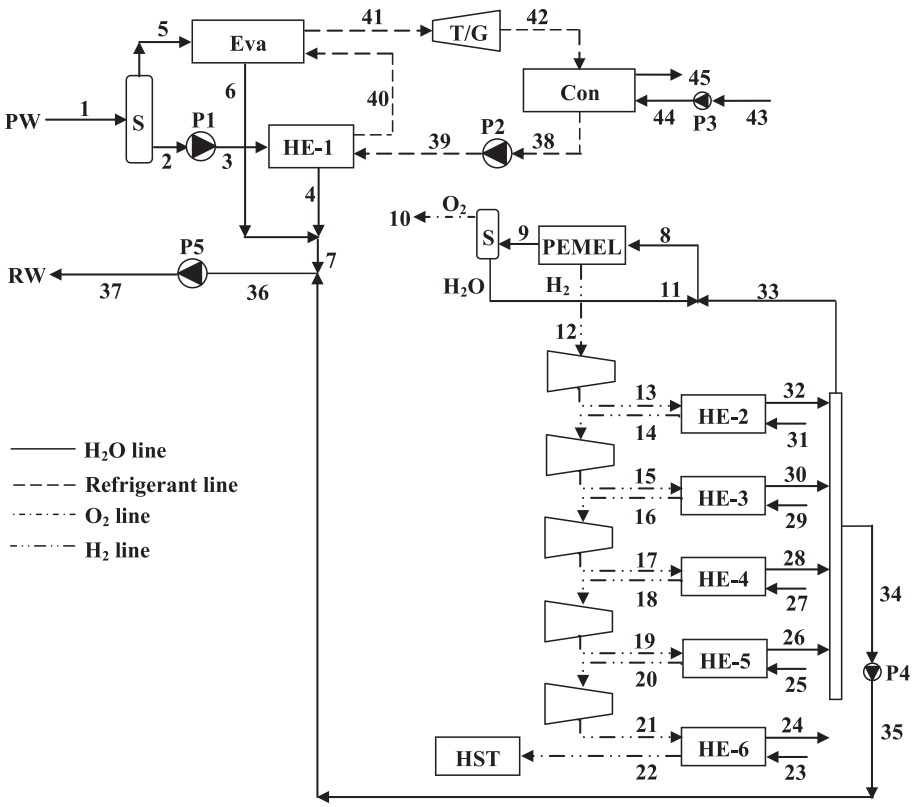

Fig. 1. Schematic of hybrid ORC-PEMEL system.

on the geothermal source temperature. Yilmaz and Kanoglu [26] investigated the hydrogen generation via PEMEL. The required power was supplied from ORC driven by geothermal sources. The exergy efficiency of the system was reported as 23.8 %, whereas the energy efficiency was reported as 6.7 %. Han et al. [27] investigated hydrogen production via PEMEL driven by ORC with a zeotropic mixture. The exergy efficiency of the geothermal sourced system was reported as 57.39 %, with an energy efficiency of 18.9 %. Cao et al. [28] investigated hydrogen production via PEMEL driven by three geothermal power cycles: ORC, absorption power cycle (APC) and KC. The energy-exergy efficiencies were reported as 11.89–50.82 %, 13.46–48.41 %, and 11.05–49.02 % for ORC, APC and KC, respectively.

Conducting the best design, including the optimal working parameters for the geothermal-driven energy systems, is crucial. Since the input and output parameters should be evaluated together to make the best decision for the geothermal system, including power and hydrogen generation, multi-criteria decision-making (MCDM) methods are prominent to determine the optimal design. In the literature, limited studies were conducted on this subject. Hasani et al. [29] investigated the ORC configurations integrated with the PEMEL. The best configuration was determined by several MCDM methods such as the Linear Programming Technique for Multidimensional Analysis of Preference (LINMAP), Technique for Order of Preference by Similarity to Ideal Solution (TOPSIS), Shannon Entropy (SE), Višekriterijumsko Kompromisno Rangiranje (VIKOR), and Gray Wolf Optimizer (GWO). Temperature, mass rate, and pressure difference were used as the decision parameters, whereas the exergy efficiency, power output, net present value (NPV) and hydrogen generation rate were performance parameters. Alirahmi et al. [30] investigated the optimization of green hydrogen and power generation via geothermal-driven ORC and PEMEL. Non-dominated Sorting Genetic Algorithm-II (NSGA-II) was used as the optimization tool. Mass rate and temperature were selected as optimization parameters, whereas the exergy efficiency and cost rate were selected as the objective functions. Haghghi et al. [31] investigated the optimization of poly-generation energy systems, including power and hydrogen generation driven by geothermal energy. TOPSIS method was used for the decision of the optimal system. Pressure, temperature, and mass rate were selected as the decision points, whereas the exergy efficiency to investment cost rate was selected as the objective. Zoghi and Zhao [32] investigated the optimization of geothermal-driven tri-generation systems, including ORC and PEMEL. The hybrid Genetic-Fgoalattain algorithm was used for the optimization. Geothermal fluid split ratio, mass fraction, temperature and pressure were selected as the decision points, whereas the exergy efficiency, total cost rate, total unit cost of products, and payback period were selected as the objective parameters.

Li et al. [33] investigated the multi-objective optimization of a novel geothermal-driven poly-generation system, including KC and PEMEL. LINMAP and TOPSIS were used to determine the optimal system. Mass rate, temperature, pressure and pressure ratio were used as the decision variables, whereas the energy efficiency, exergy efficiency, mass rate of the products, power generation, heat generation, unit costs of products and payback period were used as the performance indicators. Hekmatshoar et al. [34] investigated the optimization of the geothermal-driven poly-generation system, including ORC and PEMEL. The TOPSIS method was used to determine the best design for the proposed system. Temperature and pressure terms were selected as the decision variables, whereas the exergy efficiency and costs were selected as the performance parameters.

As in the literature, the performance parameters, such as efficiency and economic parameters, such as the cost, are very valuable to make a decision on the optimal system design. However, these indicators do not directly meet the requirements for the sustainability of the resources at the decision point. The sustainability index (SI), dependent on the exergy efficiency, is an alternative indicator in this way [35]. In the long run of the energy systems, SI, ranging between 0 and infinity, is very important for the components and overall system [36]. Also, SI is a useful tool to understand the effects of the handled parameters on the

Table 1
Technical properties of the geothermal wells.

Well	Depth (m)	Temperature (°C)	Mass rate (kg/s)
E-6	169	157	70
E-8	205	161	50
E-9	208	98	60
E-10	2000	Re-injection well (RW)	
E-11	502	99	35
EJ-1	725	162	72
EJ-3	424	151	50
EJ-4	588	152	65
EJ-5	603	152	60
Overall	–	*133.5*	*462*

system [37]. Since SI is measured by exergy efficiency, it depends on the exergy destruction caused by the entropy generation. Therefore, it is offered to be higher than the value of 1 as much as possible [38]. When the investment issues are in question, the cost issues become prominent. Moreover, it is the most important parameter from the investor's point of view. In this regard, SI is insufficient since it does not include economic views. Therefore, a coupled parameter including economic and thermodynamic performance indicators would be more attractive for optimal designs.

In this study, a new index named the economic sustainable index (EcoSI) was derived for a sensitive decision for the sustainable energy resource in this study. EcoSI was obtained to improve the sustainability of a new geothermal-driven hybrid system considering the thermodynamic performance indicator (exergetic efficiency) and economic indicator (exergoeconomic). This new geothermal-driven hybrid system was formed of ORC and PEMEL subsystems. The new system aimed to improve the sustainability of issued geothermal resources. The proposed system was later optimized by efficiency analysis technique with output satisficing (EATWOS) using SI and EcoSI indexes as the outputs.

2. Material and methods

In this study, a new design was formed to improve and measure the sustainability of geothermal energy use by hybridizing hydrogen and power generation and an arrangement of the re-injection of the geothermal fluid. The flow diagram of the system is given in Fig. 1. The hybrid system includes an ORC for power generation, a PEMEL for hydrogen generation, and a liquefying system.

The designed system is driven by geothermal resources, including eight production wells (PW) and one re-injection well (RW), located in Simav Graben, Kutahya, Turkey. The total mass rate of the geothermal fluid is 462 kg/s, whereas 10 percent of this mass is in the vapor form. The details of the wells are given in Table 1 [39,40].

According to the designed system given in Fig. 1, the liquid (point 2) and vapor phases (point 5) of the geothermal fluid (H_2O) are separated in the separator (S). The liquid phase is used for the pre-heating of the refrigerant (points 39–40), whereas the vapor phase is used for the evaporation of the refrigerant (points 40–41). The evaporated and pressurized refrigerant generates power in the turbine-generator group (T/G) at point 41. The used refrigerant vapor is then condensed (point 38) in the condenser (Con) by the cooling water (points 43–45). Some of the generated power is used in PEMEL to produce H_2 and O_2, and some is used to liquefy the H_2. Five compressors with intercoolers are used in the liquefying process (points 12–21). In PEMEL, the required heat for H_2O is obtained by the internal heat generation whereas the required heat of make-up H_2O (point 33) is supplied from the intercoolers (HE-2 to 6) of the compressors (points 13–22). The heated excess water (point 34) is then mixed with the re-injected geothermal fluid to improve the sustainability of the geothermal resources (point 37). The proposed system is analyzed and optimized following the flowchart in Fig. 2.

According to the Fig. 2, different designs are formed to determine the optimum solution considering different parameters. In this regard, ORC

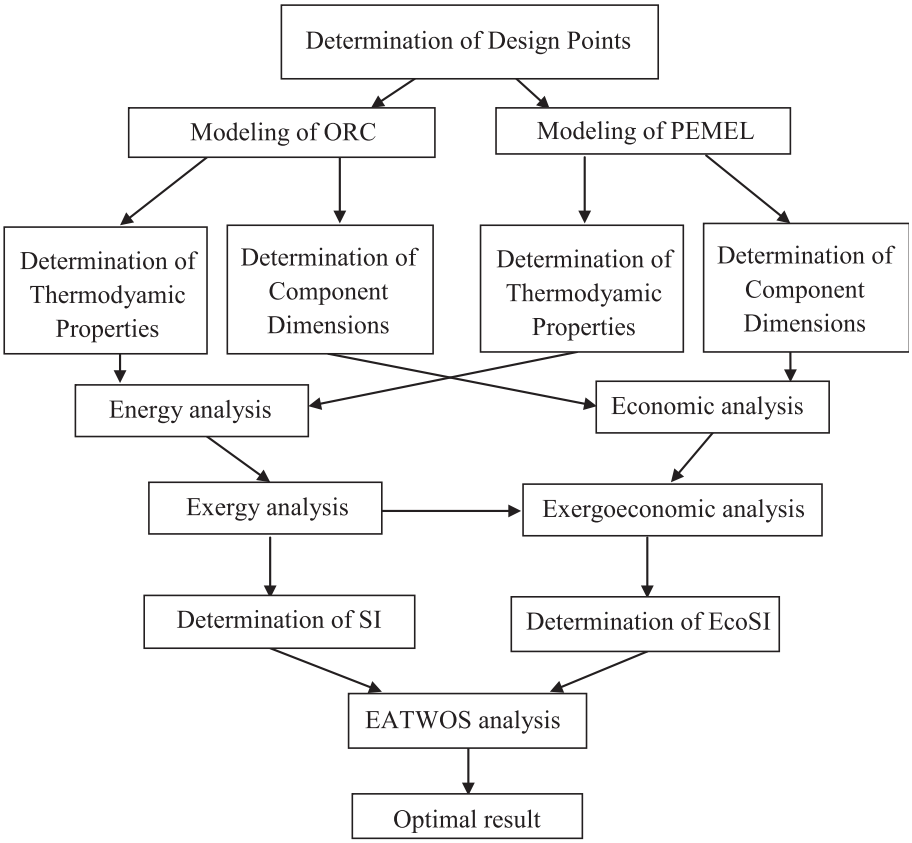

Fig. 2. Flowchart of the modeling and optimization.

Table 2
The parameters of performed designs.

T_4 (°C)		T_{41} (°C)		P_{41} (kPa)		J (A/m^2)		FR (%)	
Index	**Value**	**Index**	**Value**	**Index**	**Value**	**Index**	**Value**	**Index**	**Value**
1	110	1	95	1	1400	1	1000	1	10
2	105	2	100	2	1500	2	2000	2	30
3	100	3	105	3	1600	3	3000	3	50
4	95	4	110	4	1700	4	4000	4	70
		5	115	5	1800	5	5000		
		6	120	6	1900				
				7	1950				
				8	2000				
				9	2100				
				10	2150				
				11	2200				
				12	2300				
				13	2350				
				14	2400				
				15	2500				
				16	2600				
				17	2700				
				18	2800				

Table 3
Governing equations of Eva, Con and HE-1 for heat transfer [44].

Component	h (W/m^{2}K) or Nu
Eva Con	$h_d = 0.926 \cdot k_l \cdot \left(\frac{\rho_l g(\rho_l - \rho_g)}{\Gamma \mu_l}\right)^{1/3}$ $\Gamma = \left(\frac{\dot{m}}{n_{pipe} \cdot \pi \cdot d_o}\right)$ $Nu_i = 5 + 0.015 Re^m Pr^n$ $n = \frac{1}{3} + 0.5^{(-0.6Pr)}$ $m = 0.88 - \frac{0.24}{4+Pr}$
HE-1	$Nu_d = JRePr^{1/3}\left(\frac{\mu}{\mu_0}\right)^{0.14}$ $J = e^a a = \left(\frac{\begin{pmatrix} -0.512\ln(Re)^5 + 17.8\ln(Re)^4 \\ -731.6\ln(Re)^3 + 4331\ln(Re)^2 \\ -5957\ln(Re) - 6109 \end{pmatrix}}{\begin{pmatrix} \ln(Re)^3 + 1037\ln(Re)^2 \\ -7684\ln(Re) - 15370 \end{pmatrix}}\right)$ $Nu_i = 5 + 0.015 Re^m Pr^n$ $n = \frac{1}{3} + 0.5^{(-0.6Pr)}$ $m = 0.88 - \frac{0.24}{4+Pr}$

Table 4
Governing equations of Eva, Con and HE-1 for pressure drop.

Component	Pressure drop, ΔP (Pa)
Eva Con	$\Delta P_{shell} = f\frac{L}{d_s}\frac{\rho V^2}{2}$ $f_{Con} = \frac{0.316}{Re^{0.25}}$ $\Delta P_{tube} = \left(f\frac{L}{d_i} + 2.5\right)\frac{\rho V^2}{2}$ $f = f_{HE-1} = \frac{64}{Re}$ $0.316Re^{-0.25}$ $Re < 20000$ $0.184Re^{-0.20}$ $Re \geqslant 20000$
HE-1	$\Delta P_{shell} = 8 \cdot J_F \cdot \left(\frac{d}{d_e}\right)\frac{L}{e}\frac{\rho V_G^2}{2}\left(\frac{\mu}{\mu_0}\right)^{-0.14}$ $J_F = e^b b = \left(\frac{\begin{pmatrix} -0.1292\ln(Re)^5 + 6.332\ln(Re)^4 \\ -136.3\ln(Re)^3 + 1257\ln(Re)^2 \\ -5232\ln(Re) - 7703 \end{pmatrix}}{\begin{pmatrix} \ln(Re)^3 + 45.12\ln(Re)^2 \\ -604.9\ln(Re) - 2071 \end{pmatrix}}\right)$ $d_e = \frac{d_{shell}^2 - 1124 \cdot d_o^2}{d_{shell} + 1124 \cdot d_o} V_G = \left(\frac{\dot{m}}{\rho \cdot A_s}\right) A_s = \frac{(S_T - d_o) \cdot e \cdot d_s}{S_T}$ $\Delta P_{tube} = \left(f\frac{L}{d_i} + 2.5\right)\frac{\rho V^2}{2}$

and PEMEL subsystems are parametrically analyzed to determine the thermodynamic properties and dimensions of the designs. Energy and exergy analyses are conducted using the thermodynamic properties, whereas economic evaluation is conducted using the determined dimensions (sizes) of components of the systems. Exergoeconomic analysis is conducted using the results of economic and thermodynamic analyses. The sustainability index (SI) is determined via the exergy results, whereas the economic sustainability index (EcoSI) is determined via the exergoeconomic results. Finally, EATWOS analysis is conducted using SI and EcoSI as the outputs to perform the optimal solution.

Table 5
PEMEL Characteristics [45–51].

Parameter	Unit	Value
P_{H_2}	atm	1
P_{O_2}	atm	1
T_0	(K)	298.15
T	(K)	353
Symmetrical factor, α	–	0.5
Number of electrons per reaction, z	–	2
Universal gas constant, R	(J/mol·K)	8.3145
Faraday constant, F	(C/mol)	96,486
Anode water content, λ_a	–	14
Cathode water content, λ_c	–	10
Electrolyte thickness, t	(μm)	50
Anode pre-exponential factor, J_a^{ref}	(A/m^2)	$3.6 \cdot 10^{-5}$
Cathode pre-exponential factor, J_c^{ref}	(A/m^2)	10
Anode activation energy, $E_{act,a}$	(kJ/mol)	76
Cathode activation energy, $E_{act,a}$ (kJ/mol)	(kJ/mol)	18

Table 6
Governing equations of HE-2 to HE-6.

Component	h (W/m^{2}K) or Nu
HE-2 HE-3 HE-4 HE-5 HE-6	$h_{H_2} = (St \cdot Pr^{2/3}) \cdot \left(\frac{k_{H_2}}{d_h}\right) \cdot Re \cdot Pr^{1/3} Nu_{H_2O} = 3.66\frac{1}{U} = \frac{1}{h_{H_2O}}\frac{A_o}{A_i} + \frac{1}{\eta \cdot h_{H_2}}$ $\eta = \eta_{fin}\frac{A_{fin}}{A_{total}} + \frac{A_{base}}{A_{total}}$ ΔP (Pa) $\Delta P_{fin} = \frac{\left(\frac{\dot{m}}{A_{min}}\right)}{\rho_{H_2}}\left\{\begin{matrix}\left[\zeta_d + 1 - \left(\frac{A_{min}}{A_{front}}\right)^2\right] + f\frac{A_{min}}{A_{total}} \\ -\left[1 - \zeta_g - \left(\frac{A_{min}}{A_{front}}\right)^2\right]\end{matrix}\right\}$ $\Delta P_{tube} = f\frac{L}{d}\frac{\rho V^2}{2}$

2400 designs were performed for the different working parameters. The designs were formed considering the available working conditions and the properties of geothermal resources. In this regard, the cooling water inlet temperature (T_{43}) was assumed as 15 °C, whereas the outlet temperature (T_{45}) was set to 25 °C, taking a temperature difference of 5 °C for an effective heat transfer [35]. The inlet temperature of compressors (except for C-1) and the outlet temperature of Con (T_{38}) were respectively set to 25 °C and 20 °C for the same reason. The liquefied

Table 7
Finned type heat exchanger characteristics.

Parameter	Value
Outer pipe diameter, d_o (m)	0.011
Inner pipe diameter, d_i (m)	0.008
Hydraulic diameter, d_h (m)	0.0036
A_{min}/A_{front}	0.534
Compactness factor, β (m^2/m^3)	589
A_{fin}/A_{total}	0.839
Fin thickness (m)	0.00033
Fin pitch (pcs/m)	315

hydrogen pressure (P_{22}) was set to 70 MPa in accordance with the standards. Design numbering was prepared in the form of *T_4-T_{41}-P_{41}-J-Feeding* Rate (FR). The parameters of the designs are given in Table 2.

The other parameters of the system were taken as constant where $T_1 = T_2 = T_3 = T_5 = 133.5$ °C, $T_{38} = 20$ °C, $P_{38} = 304$ kPa, $T_{43} = 15$ °C, $T_{45} = 25$ °C, $T_8 = T_9 = T_{10} = T_{11} = T_{12} = T_{24} = T_{26} = T_{28} = T_{30} = T_{32} = T_{33} = T_{34} = 80$ °C, $T_{23} = T_{25} = T_{27} = T_{37} = T_{31} = 15$ °C, $P_8 = P_9 = P_{10} = P_{11} = P_{12} = P_{23} = P_{25} = P_{27} = P_{37} = P_{31} = 1$ atm. All the other parameters were determined according to the thermodynamic laws. As an example, when mention about Design 3–4-2–5-3, it means $T_4 = 100$ °C, $T_{41} = 110$ °C, $P_{41} = 1800$ kPa, $J = 5000$ A/m^2, $FR = 50$ %. The calculations were analytically and manually handled one by one for the each 2400 design via the codes prepared in Excel software.

2.1. Modeling of ORC

ORC system is mainly formed by turbine-generator group (T/G), condenser (Con), pumps (P1, P2, P3), pre-heater (HE-2) and evaporator (Eva). The working fluid was selected as R600a due to its lower ozone depletion of nearly zero and global warming potential of approximately 20 [41]. R600a is also commonly used in power generation and various energy systems depending on the available thermodynamic properties and its easy attainability in the market [42,43]. The efficiencies (η) of pumps and T/G were introduced into modeling as 0.8. The efficiency of heat exchangers (shell-and-tube type) was assumed to be 0.98, considering the losses from the surfaces under the worst conditions. In terms of heat transfer coefficient (U), correction factor (F) and logarithmic mean temperature difference (ΔT_{lm}), the required heat transfer area (A) of the heat exchangers is determined as:

$$A = \frac{Q}{\frac{1}{\frac{d_o}{d_i}\frac{1}{h_i}+\ln\left(\frac{d_o}{d_i}\right)\frac{d_o}{2\cdot k}+\frac{1}{h_d}}\cdot F\cdot\Delta T_{lm}} \quad (1)$$

The convective heat transfer coefficients are obtained from the related Nusselt number (Nu) or the empirical equations as given in Table 3 [44]. In all the equations, subscripts i and o refer to inlet or inner and outlet or outer, respectively.

The heat conduction of the pipes with the inner diameter (d_i) of 0.019 m and outer diameter (d_o) of 0.025 m is 54 W/mK. The used heat exchanger's shell diameter (d_i), including 1124 pipes in two passes with a length (L) of 3 m, is 1.159 m. The distance (S_T) between the centers of the pipes is 0.032 m, whereas the distance with baffles is 0.35 m [44]. The pressure drops in the heat exchangers were also introduced to calculation in the designing stage. The flow characteristics are given in Table 4 [44].

According to Tables 2 and 3, the required pump power is determined as follows:

Table 8
Energy Balances of the Hybrid System.

Component		Energy Balance	
ORC		S	$\dot{Q}_S = (\dot{m}\cdot h)_5 + (\dot{m}\cdot h)_2 - (\dot{m}\cdot h)_1$
	Eva		$\dot{Q}_{Eva} = (\dot{m}\cdot h)_6 + (\dot{m}\cdot h)_{41} - (\dot{m}\cdot h)_5 - (\dot{m}\cdot h)_{40}$
	HE-1		$\dot{Q}_{HE-1} = (\dot{m}\cdot h)_4 + (\dot{m}\cdot h)_{40} - (\dot{m}\cdot h)_3 - (\dot{m}\cdot h)_{39}$
	Con		$\dot{Q}_{Con} = (\dot{m}\cdot h)_{38} + (\dot{m}\cdot h)_{45} - (\dot{m}\cdot h)_{42} - (\dot{m}\cdot h)_{44}$
	T/G		$\dot{Q}_{T/G} = \dot{W}_{T/G} + (\dot{m}\cdot h)_{42} - (\dot{m}\cdot h)_{41}$
	P1		$\dot{Q}_{P1} = (\dot{m}\cdot h)_3 - (\dot{m}\cdot h)_2 - \dot{W}_{P1}$
	P2		$\dot{Q}_{P2} = (\dot{m}\cdot h)_{39} - (\dot{m}\cdot h)_{38} - \dot{W}_{P2}$
	P3		$\dot{Q}_{P3} = (\dot{m}\cdot h)_{44} - (\dot{m}\cdot h)_{43} - \dot{W}_{P3}$
	Overall		$\eta_{ORC} = \frac{\dot{W}_{T/G} - \dot{W}_{P1} - \dot{W}_{P2} - \dot{W}_{P3}}{(\dot{m}\cdot h)_1 + (\dot{m}\cdot h)_{43} - (\dot{m}\cdot h)_4 - (\dot{m}\cdot h)_6 - (\dot{m}\cdot h)_{45}}$
PEMEL	S		$\dot{Q}_S = (\dot{m}\cdot h)_{10} + (\dot{m}\cdot h)_{11} - (\dot{m}\cdot h)_9$
	PEMEL		$\dot{Q}_{PEMEL} = (\dot{m}\cdot h)_9 + (\dot{m}\cdot h)_{12} - (\dot{m}\cdot h)_8 - \dot{W}_{PEMEL}$
	C-1		$\dot{Q}_{C-1} = (\dot{m}\cdot h)_{13} - (\dot{m}\cdot h)_{12} - \dot{W}_{C-1}$
	C-2		$\dot{Q}_{C-2} = (\dot{m}\cdot h)_{15} - (\dot{m}\cdot h)_{14} - \dot{W}_{C-2}$
	C-3		$\dot{Q}_{C-3} = (\dot{m}\cdot h)_{17} - (\dot{m}\cdot h)_{16} - \dot{W}_{C-3}$
	C-4		$\dot{Q}_{C-4} = (\dot{m}\cdot h)_{19} - (\dot{m}\cdot h)_{18} - \dot{W}_{C-4}$
	C-5		$\dot{Q}_{C-5} = (\dot{m}\cdot h)_{21} - (\dot{m}\cdot h)_{20} - \dot{W}_{C-5}$
	HE-2		$[(\dot{m}\cdot h)_{14} - (\dot{m}\cdot h)_{13}]\cdot 0.98 = (\dot{m}\cdot h)_{32} - (\dot{m}\cdot h)_{31}$
	HE-3		$[(\dot{m}\cdot h)_{16} - (\dot{m}\cdot h)_{15}]\cdot 0.98 = (\dot{m}\cdot h)_{30} - (\dot{m}\cdot h)_{29}$
	HE-4		$[(\dot{m}\cdot h)_{18} - (\dot{m}\cdot h)_{17}]\cdot 0.98 = (\dot{m}\cdot h)_{28} - (\dot{m}\cdot h)_{27}$
	HE-5		$[(\dot{m}\cdot h)_{20} - (\dot{m}\cdot h)_{19}]\cdot 0.98 = (\dot{m}\cdot h)_{26} - (\dot{m}\cdot h)_{25}$
	HE-6		$[(\dot{m}\cdot h)_{22} - (\dot{m}\cdot h)_{21}]\cdot 0.98 = (\dot{m}\cdot h)_{24} - (\dot{m}\cdot h)_{23}$
	P4		$\dot{Q}_{P4} = (\dot{m}\cdot h)_{35} - (\dot{m}\cdot h)_{34} - \dot{W}_{P4}$
	P5		$\dot{Q}_{P5} = (\dot{m}\cdot h)_{37} - (\dot{m}\cdot h)_{36} - \dot{W}_{P5}$
	Overall		$\eta_{PEMEL} = \frac{(\dot{m}\cdot h)_{H_2} + (\dot{m}\cdot h)_{O_2}}{\dot{W}_{PEMEL} + \sum \dot{W}_P + \sum \dot{W}_C + \sum_{23}^{31}(\dot{m}\cdot h)_i}$
Hybrid System		$\eta = \frac{\dot{W}_{T/G} - \dot{W}_{PEMEL} - \sum \dot{W}_P - \sum \dot{W}_C + (\dot{m}\cdot h)_{H_2} + (\dot{m}\cdot h)_{O_2}}{(\dot{m}\cdot h)_1 + (\dot{m}\cdot h)_{43} - (\dot{m}\cdot h)_{37} - (\dot{m}\cdot h)_{45} + \sum_{23}^{31}(\dot{m}\cdot h)_i}$	

Table 9
Exergy balances of the hybrid system.

Component	Exergy Balance		
		ORC	S	$\dot{E}x_{d,S} = (\dot{m}\cdot\psi)_1 - (\dot{m}\cdot\psi)_5 - (\dot{m}\cdot\psi)_2 - \left(1-\frac{T}{T_0}\right)\dot{Q}_S$
	Eva		$\dot{E}x_{d,Eva} = (\dot{m}\cdot\psi)_5 + (\dot{m}\cdot\psi)_{40} - (\dot{m}\cdot\psi)_6 - (\dot{m}\cdot\psi)_{41} - \left(1-\frac{T}{T_0}\right)\dot{Q}_{Eva}$
	HE-1		$\dot{E}x_{d,HE-1} = (\dot{m}\cdot\psi)_3 + (\dot{m}\cdot\psi)_{49} - (\dot{m}\cdot\psi)_4 - (\dot{m}\cdot\psi)_{40} - \left(1-\frac{T}{T_0}\right)\dot{Q}_{HE-1}$
	Con		$\dot{E}x_{d,Con} = (\dot{m}\cdot\psi)_{42} + (\dot{m}\cdot\psi)_{44} - (\dot{m}\cdot\psi)_{38} - (\dot{m}\cdot\psi)_{45} - \left(1-\frac{T}{T_0}\right)\dot{Q}_{Con}$
	T/G		$\dot{E}x_{d,T/G} = (\dot{m}\cdot\psi)_{41} - (\dot{m}\cdot\psi)_{42} - \dot{W}_{T/G} - \left(1-\frac{T}{T_0}\right)\dot{Q}_{T/G}$
	P1		$\dot{E}x_{d,P1} = (\dot{m}\cdot\psi)_2 - (\dot{m}\cdot\psi)_3 + \dot{W}_{P1} - \left(1-\frac{T}{T_0}\right)\dot{Q}_{P1}$
	P2		$\dot{E}x_{d,P2} = (\dot{m}\cdot\psi)_{38} - (\dot{m}\cdot\psi)_{39} + \dot{W}_{P2} - \left(1-\frac{T}{T_0}\right)\dot{Q}_{P2}$
	P3		$\dot{E}x_{d,P2} = (\dot{m}\cdot\psi)_{43} - (\dot{m}\cdot\psi)_{44} + \dot{W}_{P3} - \left(1-\frac{T}{T_0}\right)\dot{Q}_{P3}$
	Overall		$\varepsilon_{ORC} = \frac{\dot{W}_{T/G} - \dot{W}_{P1} - \dot{W}_{P2} - \dot{W}_{P3}}{(\dot{m}\cdot\psi)_1 + (\dot{m}\cdot\psi)_{43} - (\dot{m}\cdot\psi)_4 - (\dot{m}\cdot\psi)_6 - (\dot{m}\cdot\psi)_{45}}$
PEMEL	S		$\dot{E}x_{d,S} = (\dot{m}\cdot\psi)_9 - (\dot{m}\cdot\psi)_{10} - (\dot{m}\cdot\psi)_{11} - \left(1-\frac{T}{T_0}\right)\cdot\dot{Q}_S$
	PEMEL		$\dot{E}x_{d,PEMEL} = (\dot{m}\cdot\psi)_8 - (\dot{m}\cdot\psi)_9 - (\dot{m}\cdot\psi)_{12} - \left(1-\frac{T}{T_0}\right)\cdot\dot{Q}_{PEMEL} + \dot{W}_{PEMEL}$
	C-1		$\dot{E}x_{d,C-1} = (\dot{m}\cdot\psi)_{12} - (\dot{m}\cdot\psi)_{13} - \left(1-\frac{T}{T_0}\right)\cdot\dot{Q}_{C-1} + \dot{W}_{C-1}$
	C-2		$\dot{E}x_{d,C-2} = (\dot{m}\cdot\psi)_{14} - (\dot{m}\cdot\psi)_{15} - \left(1-\frac{T}{T_0}\right)\cdot\dot{Q}_{C-2} + \dot{W}_{C-2}$
	C-3		$\dot{E}x_{d,C-3} = (\dot{m}\cdot\psi)_{16} - (\dot{m}\cdot\psi)_{17} - \left(1-\frac{T}{T_0}\right)\cdot\dot{Q}_{C-3} + \dot{W}_{C-3}$
	C-4		$\dot{E}x_{d,C-4} = (\dot{m}\cdot\psi)_{18} - (\dot{m}\cdot\psi)_{19} - \left(1-\frac{T}{T_0}\right)\cdot\dot{Q}_{C-4} + \dot{W}_{C-4}$
	C-5		$\dot{E}x_{d,C-5} = (\dot{m}\cdot\psi)_{20} - (\dot{m}\cdot\psi)_{21} - \left(1-\frac{T}{T_0}\right)\cdot\dot{Q}_{C-5} + \dot{W}_{C-5}$
	HE-2		$\dot{E}x_{d,HE3} = (\dot{m}\cdot\psi)_{13} + (\dot{m}\cdot\psi)_{31} - (\dot{m}\cdot\psi)_{14} - (\dot{m}\cdot\psi)_{32} - \left(1-\frac{T}{T_0}\right)\cdot\dot{Q}_{HE-2}$
	HE-3		$\dot{E}x_{d,HE4} = (\dot{m}\cdot\psi)_{15} + (\dot{m}\cdot\psi)_{29} - (\dot{m}\cdot\psi)_{16} - (\dot{m}\cdot\psi)_{30} - \left(1-\frac{T}{T_0}\right)\cdot\dot{Q}_{HE-3}$
	HE-4		$\dot{E}x_{d,HE5} = (\dot{m}\cdot\psi)_{17} + (\dot{m}\cdot\psi)_{27} - (\dot{m}\cdot\psi)_{18} - (\dot{m}\cdot\psi)_{28} - \left(1-\frac{T}{T_0}\right)\cdot\dot{Q}_{HE-4}$
	HE-5		$\dot{E}x_{d,HE6} = (\dot{m}\cdot\psi)_{19} + (\dot{m}\cdot\psi)_{25} - (\dot{m}\cdot\psi)_{20} - (\dot{m}\cdot\psi)_{26} - \left(1-\frac{T}{T_0}\right)\cdot\dot{Q}_{HE-5}$
	HE-7		$\dot{E}x_{d,HE7} = (\dot{m}\cdot\psi)_{21} + (\dot{m}\cdot\psi)_{23} - (\dot{m}\cdot\psi)_{22} - (\dot{m}\cdot\psi)_{24} - \left(1-\frac{T}{T_0}\right)\cdot\dot{Q}_{HE-6}$
	P4		$\dot{E}x_{d,P4} = (\dot{m}\cdot\psi)_{34} - (\dot{m}\cdot\psi)_{35} + \dot{W}_{P4} - \left(1-\frac{T}{T_0}\right)\dot{Q}_{P4}$
	P5		$\dot{E}x_{d,P5} = (\dot{m}\cdot\psi)_{36} - (\dot{m}\cdot\psi)_{37} + \dot{W}_{P5} - \left(1-\frac{T}{T_0}\right)\dot{Q}_{P5}$
	Overall		$\varepsilon_{PEMEL} = \frac{(\dot{m}\cdot\psi)_{H_2} + (\dot{m}\cdot\psi)_{O_2}}{\dot{W}_{PEMEL} + \sum\dot{W}_P + \sum\dot{W}_C + \sum_{23}^{31}(\dot{m}\cdot h)_i}$
Hybrid System	$\varepsilon_{ORC} = \frac{\dot{W}_{T/G} - \dot{W}_{PEMEL} - \sum\dot{W}_P - \sum\dot{W}_C + (\dot{m}\cdot\psi)_{H_2} + (\dot{m}\cdot\psi)_{O_2}}{(\dot{m}\cdot\psi)_1 + (\dot{m}\cdot\psi)_{43} - (\dot{m}\cdot\psi)_{37} - (\dot{m}\cdot\psi)_{45} + \sum_{23}^{31}(\dot{m}\cdot h)_i}$		

$$\dot{W}_P = \frac{\dot{m}\cdot\Delta P}{\rho\cdot\eta} \quad (2)$$

The power generation from the T/G group, using the enthalpy (h) regarding the designing parameters, is determined as follows:

$$\dot{W}_{T/G} = \dot{m}\cdot(h_{41} - h_{42})\cdot\eta \quad (3)$$

2.2. Modeling of PEMEL

The required potential (V) of PEMEL mainly includes reversible potential (V_0), ohmic overpotential Nafion electrolyte (ΔV_{ohm}), activation overpotential of the anode ($\Delta V_{act,a}$), activation overpotential of the cathode ($\Delta V_{act,c}$), and concentration overpotential (ΔV_{conc}). The anode and cathode electrodes are formed of *Pt*, whereas the electrolyte is

Table 10
Exergoeconomic balances of the hybrid system.

Component	Exergoeconomic Balance and Auxiliary Equations	
ORC	S	$\dot{C}_1+\dot{Z}_S=\dot{C}_2+\dot{C}_5;\quad \dot{Z}_{drilling}=\dot{C}_1;\quad c_2=c_5$
	Eva	$\dot{C}_5+\dot{C}_{40}+\dot{Z}_{Eva}=\dot{C}_6+\dot{C}_{41};\quad c_5=c_6$
	HE-1	$\dot{C}_3+\dot{C}_{39}+\dot{Z}_{HE-1}=\dot{C}_4+\dot{C}_{40};\quad c_3=c_4$
	Con	$\dot{C}_{42}+\dot{C}_{44}+\dot{Z}_{Con}=\dot{C}_{38}+\dot{C}_{45}$
	T/G	$\dot{C}_{41}+\dot{Z}_{T/G}=\dot{C}_{42}+\dot{C}_{W,T/G}\quad c_{41}=c_{42}\quad c_W=0.5\ \$/\mathrm{MJ}$
	P1	$\dot{C}_2+\dot{C}_{W,P1}+\dot{Z}_{P1}=\dot{C}_3$
	P2	$\dot{C}_{38}+\dot{C}_{W,P2}+\dot{Z}_{P2}=\dot{C}_{39}$
	P3	$\dot{C}_{43}+\dot{C}_{W,P3}+\dot{Z}_{P3}=\dot{C}_4;\quad c_{43}=0$
	Overall ORC	$\dot{C}_1+\sum\dot{C}_{W,P}+\sum\dot{Z}=\dot{C}_7+\dot{C}_{45}+\dot{C}_{W,T/G}$
PEMEL	S	$\dot{C}_9+\dot{Z}_S=\dot{C}_{10}+\dot{C}_{11};\quad c_{O_2}=c_{H_2}$
	PEMEL	$\dot{C}_8+\dot{C}_{W,PEMEL}+\dot{Z}_{PEMEL}=\dot{C}_9+\dot{C}_{12}$
	C-1	$\dot{C}_{12}+\dot{C}_{W,C-1}+\dot{Z}_{C-1}=\dot{C}_{13}$
	C-2	$\dot{C}_{14}+\dot{C}_{W,C-2}+\dot{Z}_{C-2}=\dot{C}_{15}$
	C-3	$\dot{C}_{16}+\dot{C}_{W,C-3}+\dot{Z}_{C-3}=\dot{C}_{17}$
	C-4	$\dot{C}_{18}+\dot{C}_{W,C-4}+\dot{Z}_{C-4}=\dot{C}_{19}$
	C-5	$\dot{C}_{20}+\dot{C}_{W,C-5}+\dot{Z}_{C-5}=\dot{C}_{21}$
	HE-2	$\dot{C}_{13}+\dot{C}_{31}+\dot{Z}_{HE-2}=\dot{C}_{14}+\dot{C}_{32};\quad c_{13}=c_{14}$
	HE-3	$\dot{C}_{15}+\dot{C}_{29}+\dot{Z}_{HE-3}=\dot{C}_{16}+\dot{C}_{30};\quad c_{15}=c_{16}$
	HE-4	$\dot{C}_{17}+\dot{C}_{27}+\dot{Z}_{HE-4}=\dot{C}_{18}+\dot{C}_{28};\quad c_{17}=c_{18}$
	HE-5	$\dot{C}_{19}+\dot{C}_{25}+\dot{Z}_{HE-5}=\dot{C}_{20}+\dot{C}_{26};\quad c_{19}=c_{20}$
	HE-6	$\dot{C}_{21}+\dot{C}_{23}+\dot{Z}_{HE-6}=\dot{C}_{22}+\dot{C}_{24};\quad c_{21}+\frac{\dot{Z}_{HST}}{\dot{E}x_{21}}=c_{22}$
	P4	$\dot{C}_{34}+\dot{C}_{W,P4}+\dot{Z}_{P4}=\dot{C}_{35}$
	P5	$\dot{C}_{36}+\dot{C}_{W,P5}+\dot{Z}_{P5}=\dot{C}_{37}$
	Overall PEMEL	$\sum\dot{C}_W+\sum\dot{Z}=\dot{C}_{10}+\dot{C}_{22}$
Overall system	$\dot{C}_1+\sum\dot{C}_W+\sum\dot{Z}=\dot{C}_{37}+\dot{C}_{45}+\dot{C}_{W,T/G}$	

Table 11
Cost functions.

Component	Cost Function	$\mathrm{CEPCI_{origin}}$	Reference year	Reference
S	$\dot{Z}_0=280.3\cdot\dot{m}^{0.67}$	596.2	2020	[58]
HE (ORC)	$\dot{Z}_0=1396\cdot A^{0.89}$	585.7	2011	[59]
HE (PEMEL)	$\dot{Z}_0=2143\cdot A^{0.514}$	567.5	2017	[60]
Con	$\dot{Z}_0=1396\cdot A^{0.89}$	585.7	2011	[59]
T/G	$\dot{Z}_0=4750\cdot W^{0.75}$	596.2	2020	[58]
P	$\dot{Z}_0=3500\cdot W^{0.41}$	596.2	2020	[58]
PEMEL	$\dot{Z}_0=1000\cdot W$	585.7	2011	[61]
C	$\dot{Z}_0=5840\cdot W^{0.82}$	603.1	2018	[62]
Drilling	$\dot{Z}_0=300\cdot(Depth)$	567.5	2017	[63]
HST	$\dot{Z}_0=4800\cdot\left(\frac{V_{H_2}}{12.5}\right)$	799.5	2023	–

formed of Nafion. The concentration overpotential can be neglected when the current density (J) is lower than 10,000 A/m^2. So, the required potential is given as [45]:

$$V=\ V_0+\Delta V_{act,a}+\Delta V_{act,c}+\Delta V_{ohm} \tag{4}$$

The reversible potential is given by the Nernst equation [46]:

$$V_0=1.23-0.9\cdot10^{-3}(T-T_0)+\frac{RT}{4F}\ln\left(P_{H_2}^2\cdot P_{O_2}\right) \tag{5}$$

where T and T_0 are the working and reference temperatures, respectively. P_{H_2} and P_{O_2} are the pressures of hydrogen at point 12 and oxygen at point 10, respectively. In terms of current density (J) and the overall ohmic resistance (R_{PEMEL}), the ohmic overpotential of an electrolyte with a thickness of t is given as [47,48]:

$$\Delta V_{ohm}=J\cdot R_{PEMEL} \tag{6}$$

$$R_{PEMEL}=\int_0^t\frac{dx}{\sigma[\lambda(x)]} \tag{7}$$

$$\sigma[\lambda(x)]=[0.5139\cdot\lambda(x)-0.326]\cdot e^{1268\left(\frac{1}{303}-\frac{1}{T}\right)} \tag{8}$$

$$\lambda(x)=\frac{\lambda_a-\lambda_c}{t}x+\lambda_c \tag{9}$$

$$J=\ J_{0,i}\cdot\left(e^{\frac{\alpha\cdot z\cdot F\cdot\Delta V_{act,i}}{RT}}-e^{\frac{(1-\alpha)\cdot z\cdot F\cdot\Delta V_{act,i}}{RT}}\right)\quad i=a,\ c \tag{10}$$

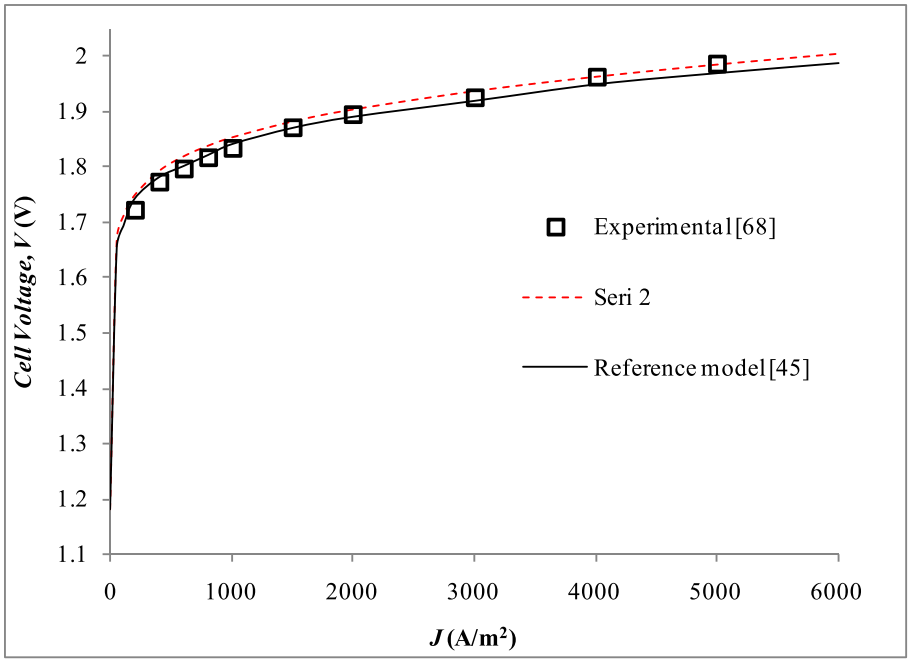

Fig. 3. Validation of the PEMEL modeling.

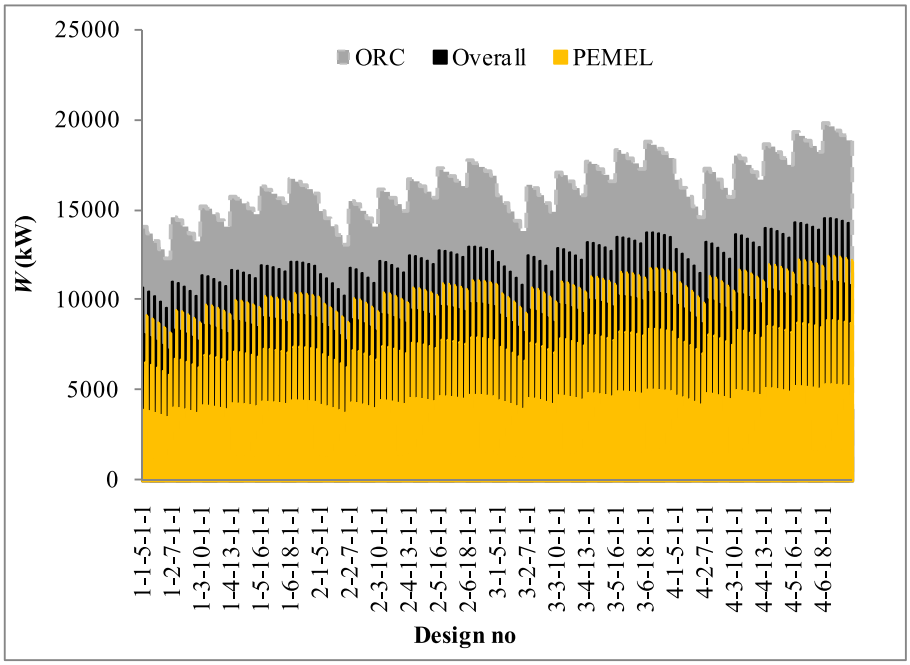

Fig. 4. Work output and requirements.

$$\Delta V_{act,i} = \frac{RT}{F}\ln\left(\frac{J}{2J_{0,i}} + \sqrt{\left(\frac{J}{2J_{0,i}}\right)^2 + 1}\right) \quad i = a,\ c \tag{11}$$

$$J_{0,i} = J_i^{ref} \cdot e^{-\frac{E_{act,i}}{RT}} \quad i = a,\ c \tag{12}$$

Detailed information about parameters used in the modeling of PEMEL is given in Table 5 [45–51].

So the generated hydrogen (NHo) and oxygen ($\dot{N}_{O_2}$) rates are given as:

$$\dot{N}_{H_2} = \frac{J}{2F} \tag{13}$$

$$\dot{N}_{O_2} = \frac{J}{4F} \tag{14}$$

The hydrogen liquefying system includes five compressors for effective working conditions with a compression ratio (r) of 3.7 [52,53]. The system also includes finned pipe-type heat exchangers to cool the hydrogen and heat the feeding water of PEMEL to improve the compressor efficiency. According to this, the required compressor power is determined as follows:

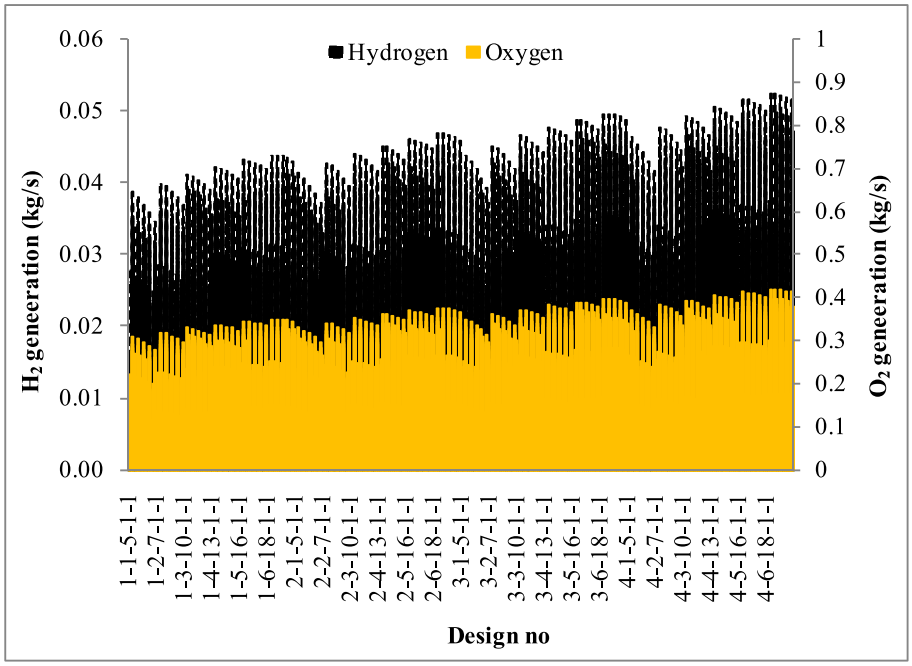

Fig. 5. H_2 and O_2 generation rates.

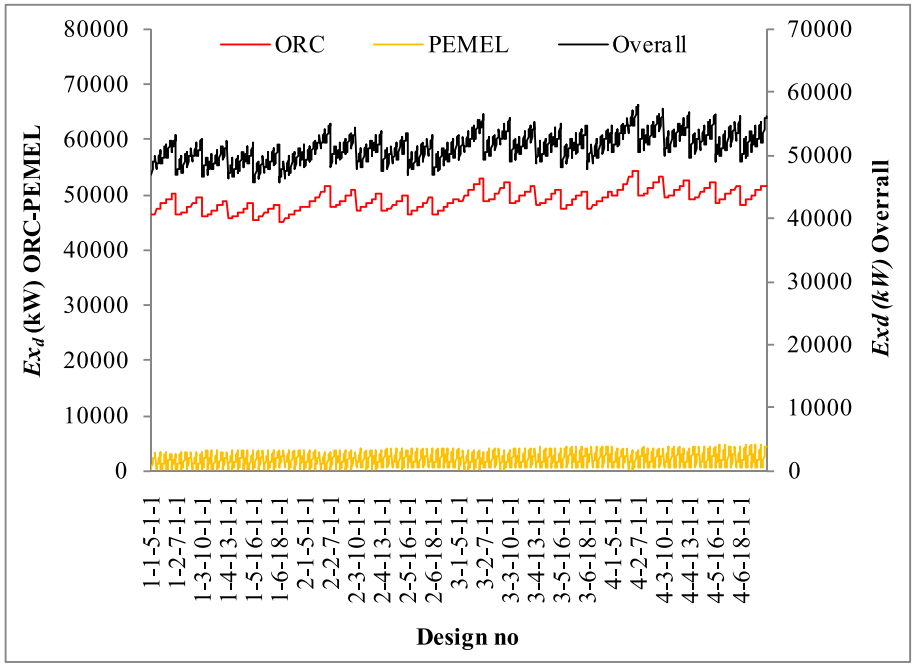

Fig. 6. The exergy destruction rates.

$$\dot{W}_C = \frac{\dot{m} C_p T}{\eta}\left[\left(\frac{P_{out}}{P_{in}}\right)^{\frac{k-1}{k}} - 1\right] \quad (15)$$

where k is the isentropic exponent (=1.4), η is the compressor efficient (=0.70), C_p is the specific heat, and $\dot{m}$ is the flow rate of the compressed hydrogen. P_{out} and P_{in} are the flow outlet and inlet pressures, respectively. The required heat transfer area is calculated similarly to the heat exchangers of ORC. The related Nusselt number (Nu) or the empirical equations are given in Table 6 [44]. In the heat exchangers, water flows in the tubes, whereas hydrogen flows over the finned tubes.

The characteristics of the used finned heat exchanger are given in Table 7 [44].

2.3. Energy, exergy and exergoeconomic analysis

Exergoeconomic analysis is conducted along with the exergy analysis, whereas the exergy analysis is conducted with the energy analysis. Concerning this, the mass, energy, and exergy balances of the k^{th} component for the steady-state conditions are given as:

$$\sum \dot{m}_{i,k} - \sum \dot{m}_{o,k} = 0 \quad (16)$$

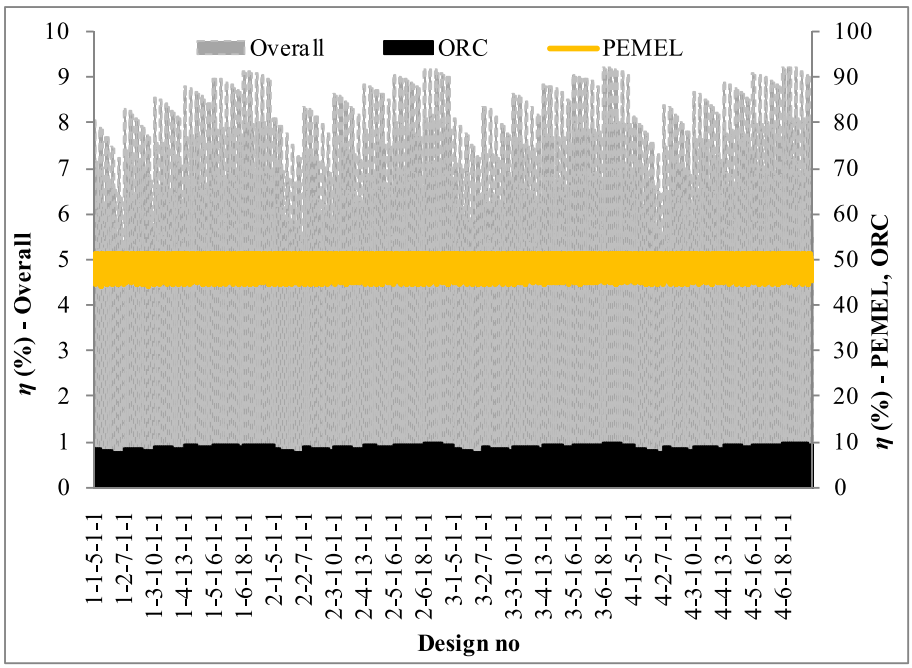

Fig. 7. The variation of energy efficiency.

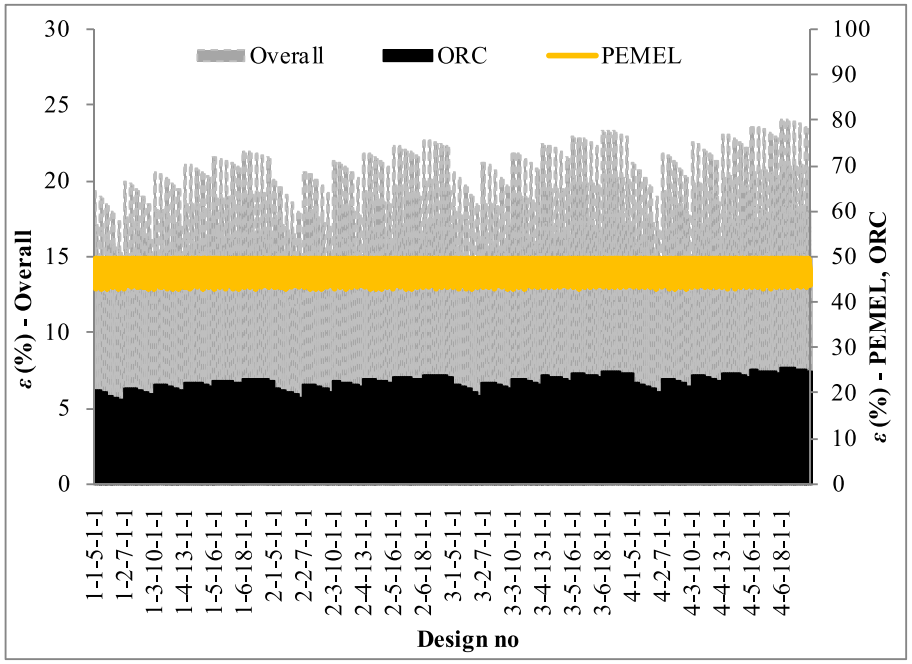

Fig. 8. The variation of exergy efficiency.

$$\dot{Q}_k - \dot{W}_k + \sum (\dot{m}\cdot h)_{i,k} - \sum (\dot{m}\cdot h)_{o,k} = 0 \tag{17}$$

$$\left(1 - \frac{T_0}{T}\right)\cdot\dot{Q}_k - \dot{W}_k + \sum (\dot{m}\cdot\psi)_{i,k} - \sum (\dot{m}\cdot\psi)_{o,k} = \dot{E}x_{d,k} \tag{18}$$

where subscripts d and 0 refer to destructed exergy and reference state, respectively. ψ refers to the specific exergy of the flow and is given as the sum of physical (ψ^{Ph}) and chemical exergy (ψ^{Ch}) terms:

$$\psi = \psi^{Ph} + \psi^{Ch} \tag{19}$$

$$\psi = ((h - h_0) - T_0(s - s_0)) + \left(\sum x\cdot ex_{Ch} + RT_0 \sum (x\ln x)\right) \tag{20}$$

where h and s are enthalpy and entropy, respectively. $\times$ is the mole fraction of each compound, and ex_{Ch} is the standard chemical exergy of the compounds. η and ε are the energy and exergy efficiencies, respectively. The energy and exergy balances of the handled system are given in Tables 8 and 9, respectively.

Accordingly, the exergoeconomic balance equations are given as [54]:

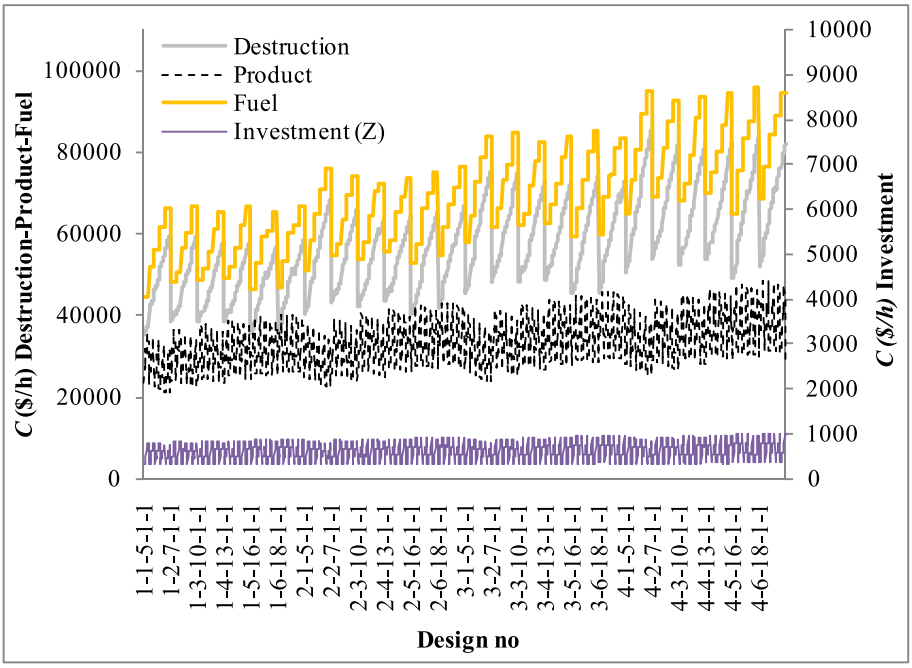

Fig. 9. Exergoeconomic costs of the hybrid system.

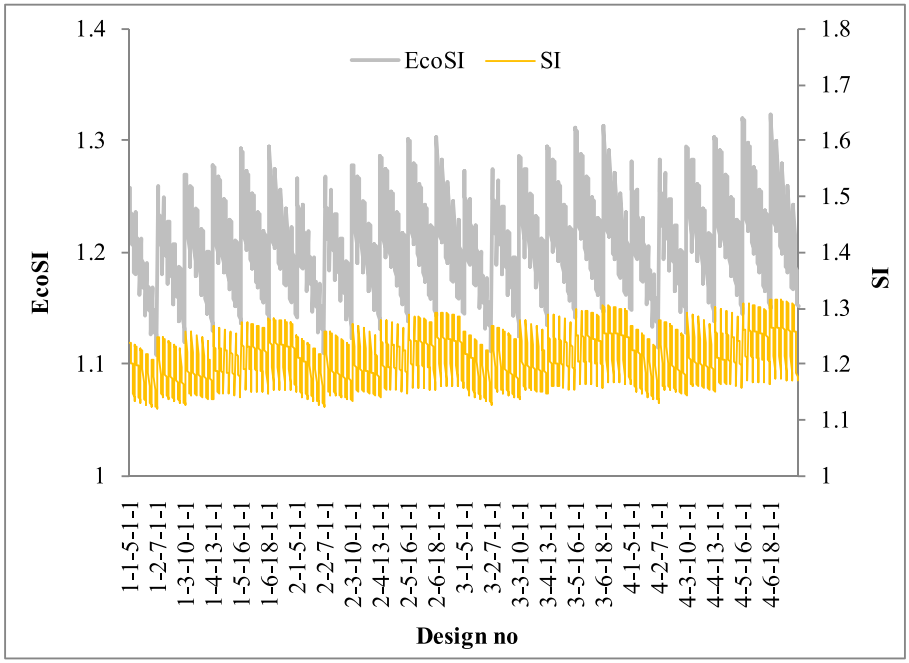

Fig. 10. The SI and EcoSI values of the designs.

$$\sum \dot{C}_{i,k} + \dot{Z}_k = \sum \dot{C}_{o,k}$$
$$\sum \left(c \cdot \dot{E}x\right)_{i,k} + \dot{Z}_k = \sum \left(c \cdot \dot{E}x\right)_{o,k} \quad (21)$$

$$\sum \dot{C}_{F,k} + \dot{Z}_k = \sum \dot{C}_{P,k}$$
$$\sum \left(c \cdot \dot{E}x\right)_{F,k} + \dot{Z}_k = \sum \left(c \cdot \dot{E}x\right)_{P,k} \quad (22)$$

$$\dot{C}_{d,k} = c_{F,k} \cdot \dot{E}x_{d,k} \quad (23)$$

$$\dot{Z}_k = \frac{\dot{Z}_0 \cdot \phi}{N} \frac{i \cdot (1+i)^n}{(1+i)^n - 1} \frac{CI}{CI_{origin}} \quad (24)$$

where the subscripts F and P refer to fuel and products of the k^{th} component, respectively. C defines cost flow, whereas c defines the specific cost. Z_0 denotes the cost of the component, whereas Z_k denotes the adjusted cost including operating and maintenance. Superscript n refers to the system's lifetime and was taken as 20 years. N is the working hours of the system per year and was taken as 8760 h. The interest rate (i) and operation and maintenance factor (φ) were taken as 10.75 % [55] and 1.06 [56]. CI (=799.5) and CI_{origin} refer to the current

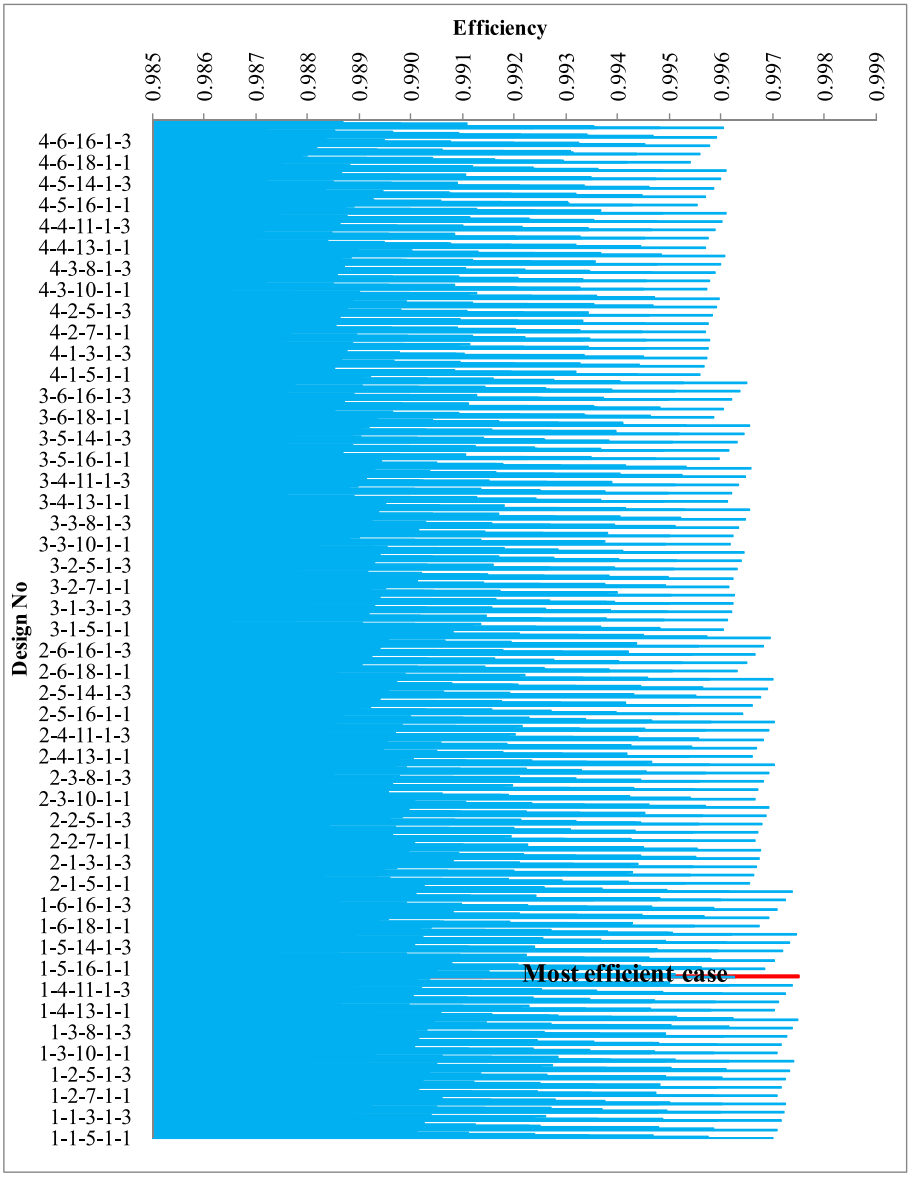

Fig. 11. EATWOS efficiency results based on SI effect.

cost index and regarding year cost index, respectively [57]. The exergoeconomic balances and the cost functions are given in Table 10 and Table 11, respectively.

2.4. Derivation of EcoSI

The sustainability index is a function of the exergy efficiency and is given by [64]:

$$SI = \frac{1}{1-\varepsilon} \tag{25}$$

Arranging Eq. (25) with the definition of exergy efficiency, the following is obtained:

$$SI = \frac{1}{1-\frac{\dot{E}x_{out}}{\dot{E}x_{in}}} = \frac{1}{\frac{\dot{E}x_i-\dot{E}x_o}{\dot{E}x_i}} = \frac{1}{\frac{\dot{E}x_d}{\dot{E}x_i}} = \frac{\dot{E}x_i}{\dot{E}x_d} = \frac{\dot{E}x_F}{\dot{E}x_d} \tag{26}$$

Substituting (22) and (23) into (26), the EcoSI is obtained as:

$$EcoSI = \frac{\sum\left(c_{P,k}-\dot{Z}_k\right)}{\sum\frac{\dot{C}_{d,k}}{c_{F,k}}} = \frac{\sum\left(C_{P,k}-\dot{Z}_k\right)}{\sum C_{d,k}} \tag{27}$$

For the overall system, (27) can be written as:

$$EcoSI = \frac{C_P-\dot{Z}}{C_d} = \frac{C_F}{C_d} \tag{28}$$

2.5. EATWOS analysis

EATWOS is successfully used for the optimization of energy systems with multi-criteria [35,41,65]. The analysis aims to maximize the outputs (y) with minimum inputs (x). The efficiency is given as [66]:

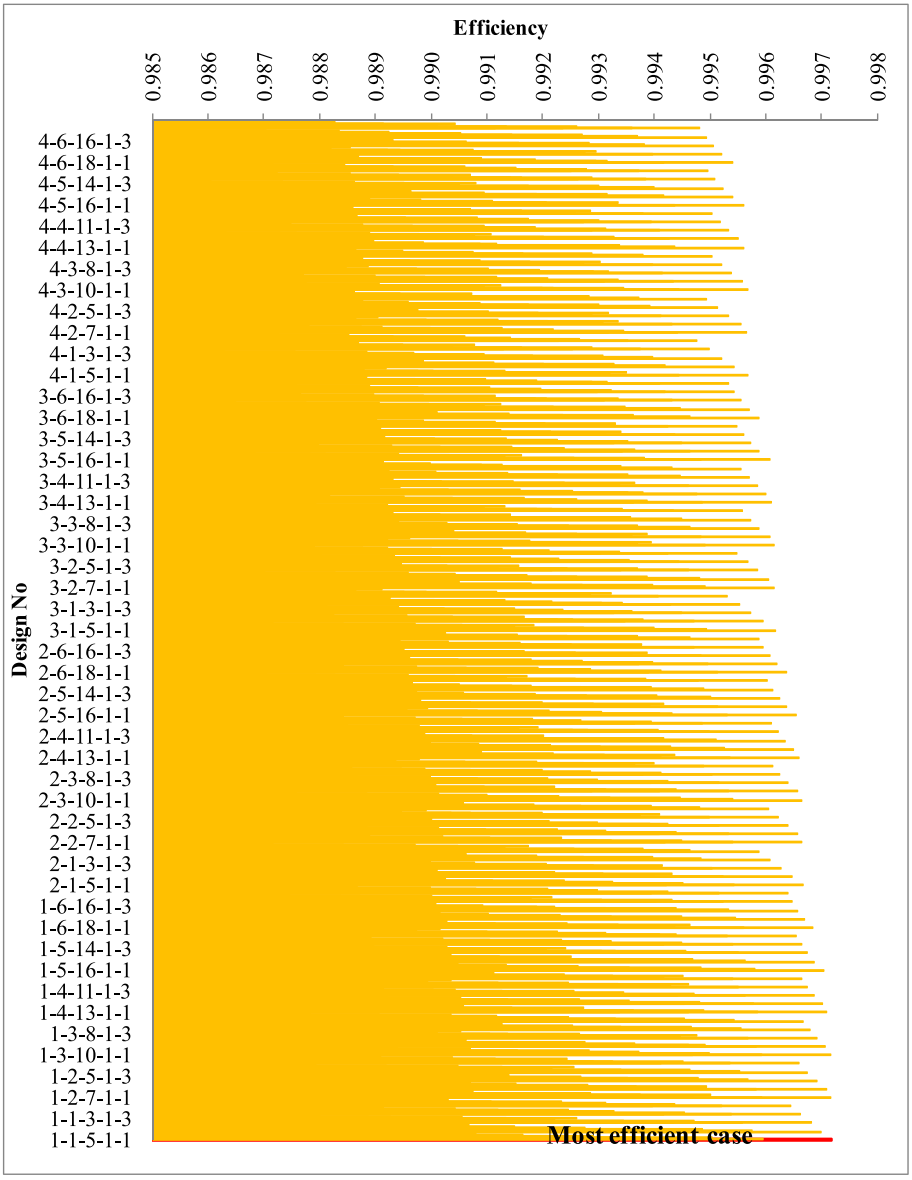

Fig. 12. EATWOS efficiency results based on EcoSI effect.

$$E_i = \frac{\sum_{j=1}^{J} \nu_j \left(1 + \frac{y_{i,j}}{\sqrt{\sum_{j}^{J} y_{i,j}^2}} - \max_i \left\{ \frac{y_j}{\sqrt{\sum_{j}^{J} x_j^2}} \right\} \right)}{\sum_{k=1}^{K} w_k \cdot \left(1 + \frac{x_{i,k}}{\sqrt{\sum_{i}^{K} x_{i,k}^2}} - \min_i \left\{ \frac{x_k}{\sqrt{\sum_{i}^{K} x_k^2}} \right\} \right)} \tag{30}$$

where ν and w are input and output parameters weights, respectively. The output values were selected as SI and EcoSI, whereas the inputs were selected as T_1- T_{37}, T_{41}, P_{41}, J, and W_{PEMEL}/W_{ORC}.

3. Results and discussions

In the study, the properties of the fluids were determined for each parameter using Refprop software [67].

3.1. Validation of PEMEL

The observed model was validated with a reference model [45] and experimental results [68] from the literature. The validation results are given in Fig. 3.

According to Fig. 3, the determination coefficient (R^2) values were obtained as 0.9997 and 0.9986 for the comparison of the reference model and experimental results, respectively. The mean absolute percentage error (MAPE) values were obtained as 0.68 % and 0.76 % for the reference model and experimental values. So, the PEMEL modeling largely agrees with the experimental results and reference model.

3.2. Energy and exergy analysis results

The generated power (ORC), required power for the hydrogen generation process (PEMEL) and net power output (Overall) were calculated, and variations for the designs are given in Fig. 4.

According to Fig. 4, the power output from the turbine group varies between 12318.18 kW and 19832.09 kW. The power generation increases with the decrease of geothermal fluid outlet temperature of ORC

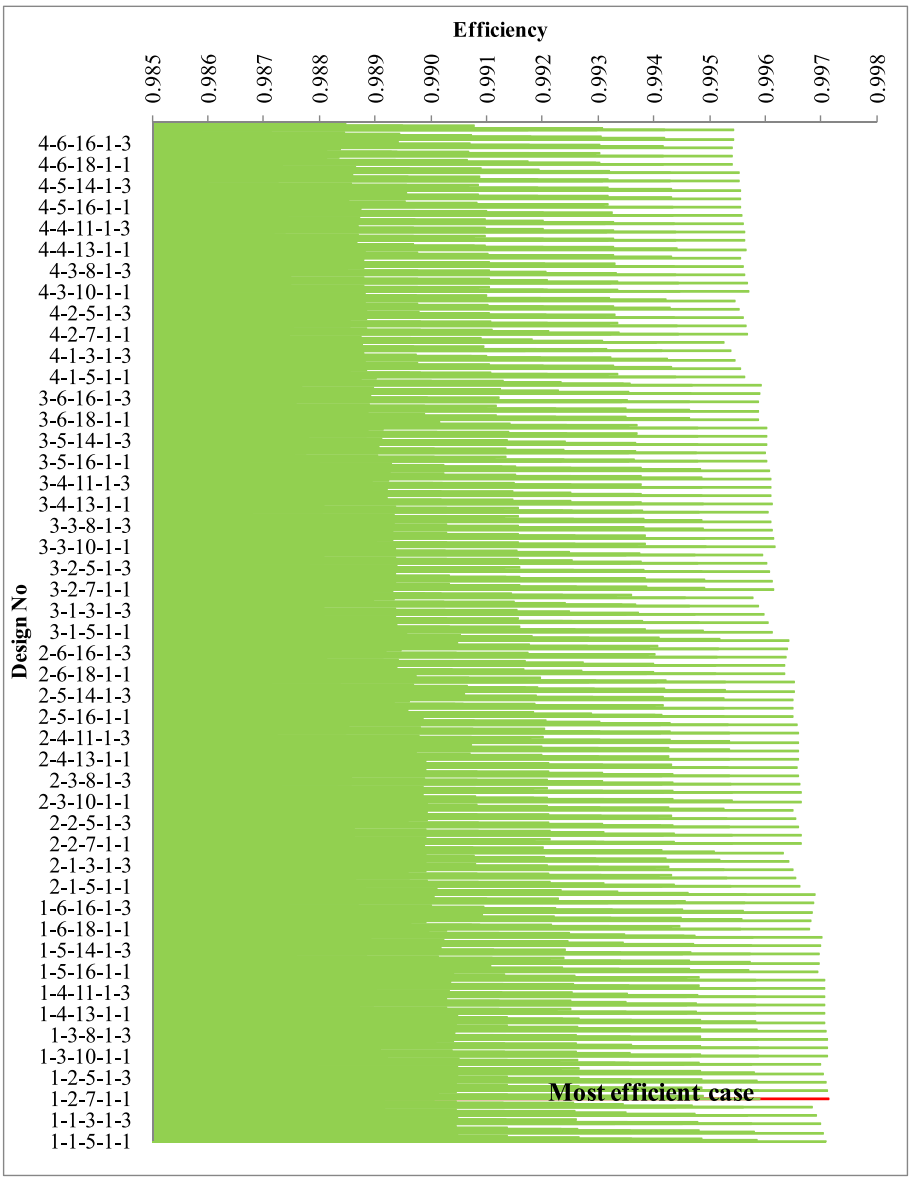

Fig. 13. EATWOS efficiency results based on combined effects.

(*T4*). The net power output from the hybrid system varies between 2606.53 kW and 14648.58 kW. The variation of the net power output largely depends on the FR and higher pressure values of the refrigerant pressure at the turbine inlet. The required hydrogen generation power, including the liquefying compressors, varies between 1193.25 kW and 12480.05 kW. This larger variation largely depends on the FR and J values since it directly affects the generated H_2 mass rate. This issue directly affects the power requirement of compressors. The variation of H_2 and O_2 generation is given in Fig. 5.

According to Fig. 5, the H_2 generation rate varies between 12318.18 kg/s and 19832.09 kg/s, whereas the O_2 rate varies between 0.004353 kg/s and 0.052464 kg/s. The FR is the most critical factor in the generation. Depending on the increase in ORC performance, H_2 generation is directly affected. So, the increase in power generation directly increases the H_2 generation rate. Also, the increase in the current density (J) decreases the generation rate due to higher potential requirements and overpotentials. These requirements and overpotential, along with the power generation capability of ORC, also directly affect the exergy destruction rates. The variation exergy destructions are given in Fig. 6.

According to Fig. 6, the exergy destruction rate of PEMEL varies between 367.68 kW and 4652.35 kW. The destruction of ORC varies between 45187.77 kW and 54329.66 kW. The overall destruction varies between 45653.36 kW and 58014.00 kW. The increases in *J* increase the exergy destruction rates. Also, the increases in turbine inlet pressure increase the exergy destruction. Depending on the irreversibilities in compressors, the causes that increase the H_2 generation rate increase the exergy destruction since the required compressor power increases. Accordingly, the energy (η) and exergy (ε) efficiency values are given in Fig. 7 and Fig. 8, respectively.

According to Fig. 7, the energy efficiency of PEMEL varies between 44.36 % and 51.37 %. The energy efficiency of ORC varies between 7.63 % and 9.76 %. The energy efficiency of overall systems varies between 4.47 % and 9.23 %. According to Fig. 8, the exergy efficiency of PEMEL varies between 42.85 % and 49.64 %. The exergy efficiency of ORC varies between 18.35 % and 25.40 %. The exergy efficiency of overall systems varies between 10.58 % and 23.99 %. The variation of the efficiency values is similar to the destruction variation since it is directly related to losses.

Table 12
Thermodynamic properties of the optimal system.

Point	T (°C)	P (kPa)	m (kg/s)	h (kJ/kg)	s (kJ/kgK)	ψ (kJ/kg)	$\dot{E}$ (kW)	$\dot{E}x$ (kW)	C ($/h)
1	133.50	300.00	462.00	777.69	2.20	125.27	359291.39	103049.99	3656.46
2	133.50	300.00	415.80	561.33	1.67	67.53	233401.01	48870.20	3365.28
3	133.50	592.65	415.80	561.64	1.67	67.84	233530.24	48999.43	3656.46
4	110.00	299.98	415.80	461.53	1.42	43.11	191904.17	38713.17	2888.87
5	133.50	300.00	46.20	2724.90	6.99	644.86	125890.38	54175.66	3730.62
6	129.96	299.98	46.20	546.24	1.63	63.56	25236.29	5246.65	361.29
7	112.00	300.00	462.00	470.00	1.44	45.02	217140.46	43897.84	3250.17
8	80.00	101.33	0.07171	335.06	1.08	18.96	24.03	4.94	463.24
9	80.00	101.33	0.06609	321.85	–	–	–	–	–
10	80.00	101.33	0.04560	321.85	6.56	4.21	14.68	5.85	1917.90
11	80.00	101.33	0.02049	335.06	1.08	18.96	6.86	1.41	463.24
12	80.00	101.33	0.00570	4722.70	55.81	65.20	26.92	673.26	2301.42
13	239.97	374.65	0.00570	7042.60	55.83	2379.44	40.14	686.46	2344.56
14	25.00	374.62	0.00570	3933.00	47.98	1610.02	22.42	682.07	2329.58
15	160.05	1385.08	0.00570	5889.80	47.98	3567.71	33.57	693.23	2365.87
16	25.00	1385.06	0.00570	3937.40	42.58	3225.32	22.44	691.28	2359.21
17	160.05	5120.89	0.00570	5915.20	42.57	5204.31	33.72	702.56	2395.59
18	25.00	5120.89	0.00570	3954.30	37.15	4860.28	22.54	700.60	2388.90
19	160.05	18933.10	0.00570	6012.50	37.15	6918.48	34.27	712.33	2425.55
20	25.00	18933.10	0.00570	4027.60	31.66	6571.02	22.96	710.35	2418.80
21	160.05	70000.00	0.00570	6403.20	31.71	8930.82	36.50	723.80	2418.80
22	25.00	70000.00	0.00570	4381.80	26.12	8577.27	24.98	721.79	2334.98
23	15.00	101.33	0.04152	63.08	0.22	0.72	2.62	2.11	0.00
24	80.00	–	0.04152	335.06	1.08	18.96	13.91	2.86	3.75
25	15.00	101.33	0.04077	63.08	0.22	0.72	2.57	2.07	0.00
26	80.00	–	0.04077	335.06	1.08	18.96	13.66	2.81	6.82
27	15.00	101.33	0.04028	63.08	0.22	0.72	2.54	2.04	0.00
28	80.00	–	0.04028	335.06	1.08	18.96	13.49	2.78	6.76
29	15.00	101.33	0.04010	63.08	0.22	0.72	2.53	2.03	0.00
30	80.00	–	0.04010	335.06	1.08	18.96	13.44	2.77	6.74
31	15.00	101.33	0.06387	63.08	0.22	0.72	4.03	3.24	0.00
32	80.00	–	0.06387	335.06	1.08	18.96	21.40	4.40	15.03
33	80.00	201.33	0.05122	335.06	1.08	18.96	17.16	3.53	0.01
34	80.00	299.29	0.17531	335.21	1.08	19.14	58.77	12.12	0.03
35	80.00	299.35	0.16132	335.21	1.08	19.14	58.77	12.12	0.03
36	111.99	300.00	462.18	469.95	1.44	45.00	217199.23	43904.65	3250.20
37	111.99	350.00	462.18	470.00	1.44	45.05	217223.57	43928.99	3305.24
38	20.00	304.00	325.95	246.88	1.16	50.07	80469.68	15752231.56	18187759.00
39	21.41	1976.27	325.95	251.61	1.17	53.84	82009.77	15753460.68	18258063.69
40	70.23	1955.80	325.95	376.37	1.56	61.52	122676.68	15755964.62	18258836.46
41	100.00	1950.00	325.95	679.00	2.38	118.60	221317.69	15774567.39	18262220.30
42	43.96	334.40	325.95	623.01	2.43	49.28	203067.29	15751973.01	18236062.77
43	15.00	101.33	2871.34	63.08	0.22	0.72	181115.79	145628.59	0.00
44	15.00	103.43	2871.34	63.08	0.22	0.72	181121.84	145634.64	52.81
45	25.00	101.33	2871.34	104.92	0.37	0.00	301261.45	143567.22	52062.71

Table 13
Energy, exergy and exergoeconomic analysis results of the optimal design.

Parameter	Component		
	ORC	PEMEL	Overall System
W (kW)	14600.32	1380.45	11103.99
Q (kW)	−129475.74	−1265.93	−130741.66
E_{in} (kW)	359291.39	14.29	359305.68
E_{out} (kW)	217140.46	98.42	217223.57
Ex_F (kW)	59152.15	1391.94	59121.01
Ex_P (kW)	14600.32	678.74	11782.73
Ex_d (kW)	46500.51	422.83	46923.34
η (%)	8.78	50.47	8.30
ε (%)	21.11	48.76	19.92
Z_K ($/h)	0.07	0.02	332.57
$c_{F,k}$ ($/MJ)	0.23	0.50	0.23
$c_{P,k}$ ($/MJ)	0.50	1.74	0.57
$C_{d,k}$ ($/h)	37904.46	754.80	38312.99
$C_{total,k}$ ($/h)	37904.53	754.83	38645.56
SI			1.249
EcoSI			1.260

3.3. Exergoeconomic analysis results

The exergoeconomic cost parameters were determined regarding destruction, product, fuel and investment for the hybrid system. The obtained results are given in Fig. 9.

According to Fig. 9, the investment exergoeconomic cost varies between 320.87 $/h and 1001.99 $/h. The destruction cost varies between 35518.44 $/h and 85296.20 $/h. The product cost varies between 20996.19 $/h and 48268.98 $/h, whereas the fuel cost varies between 44680.63 $/h and 96095.60 $/h. The cause of the variation largely depends on the higher exergy destruction rates and the sizes of the components of the systems.

3.4. EATWOS optimization

The optimization of the designed system is based on the efficiency values of the EATWOS analysis. The EATWOS analysis uses SI and EcoSI values as the outputs for the best design. In the light of exergy and exergoeconomic analysis, the SI and EcoSI were determined for all designs. The variation SI and EcoSI are given in Fig. 10.

According to Fig. 10, SI values range between 1.119 and 1.316,

Table 14
Comparative evaluation of the optimal system.

Parameter	ORC			PEMEL			***Overall System***		
	Present study	Ref [17]	Ref [19]	Present study	Ref [17]	Ref [19]	*Present study*	*Ref [17]*	*Ref [19]*
$T_{geothermal}$ (°C)	133.5	96	160	–	–	–	*133.5*	*96*	*160*
Refrigerant	R600a	R236fa	R600a	–	–	–	*R600a*	*R236fa*	*R600a*
W (kW)	14600.32	681.4	7993	−1380.45	−200	−7993	*11103.99*	*481.4*	*0.0*
$P_{T/G}$ (kPa)	1950	1000	2052	–	–	–	*1950*	*1000*	*2052*
$T_{T/G}$ (°C)	100	–	140.5	–	–	–	*1950*	*1000*	*2052*
P_{PEMEL} (kPa)	–	–	–	101.325	101.325	100	*101.325*	*101.325*	*100*
T_{PEMEL} (°C)	–	–	–	80	80	73.15	*80*	*80*	*73.15*
$\dot{m}_{H_2}$ (kg/s)	–	–	–	0.00570	0.000972	0.05269	*0.00570*	*0.000972*	*0.05269*
J (A/m^2)	–	–	–	1000	–	–	*1000*	–	–
η (%)	8.78	8.843	–	50.47	10.72	–	*8.30*	*3.32*	*8.49*
ε (%)	21.11	68.88	–	48.76	41.73	–	*19.92*	*64.86*	*38.44*
SI	–	–	–	–	–	–	*1.249*	*2.846*	*1.624*
EcoSI	–	–	–	–	–	–	*1.260*	–	–

whereas EcoSI values range between 1.108 and 1.323. EATWOS determined the efficiency values of the designs to address the best (optimal) configuration for the minimum inputs and maximum outputs. The weights were introduced into calculations as equal for each decision point. The results for the SI-based and EcoSI-based outputs are given in Figs. 11 and 12, respectively. The results for the combined outputs of SI and EcoSI are given in Fig. 13.

According to Fig. 11, the efficiency values are between 0.98297 and 0.99749. Therefore, the best design was determined as the design 1–4-8–1-1 with an efficiency score of 0.997149. In this design, the optimization variables were determined as $T_{1=}$ 133.5 °C, $T_4 = 110$ °C, $T_{37} = 111.99$ °C, $T_{41} = 110$ °C, $P_{41} = 2000$ kPa, $J = 1000$ A/m^2, $W_{PEMEL}/W_{ORC} = 10$ %. For this design, the energy and exergy efficiencies of the ORC were determined as 8.94 % and 20.47 %, respectively. The power generation rate was determined as 14.773 MW, whereas the net power generation was determined as 12.702 MW. The energy and exergy efficiencies of the PEMEL were determined as 50.44 % and 48.73 %, respectively. The hydrogen generation rate was determined as 0.005794 kg/s. The energy and exergy efficiencies of the overall system were determined as 8.45 % and 20.27 %, respectively. The investment cost (Z_k) was determined as 334.04 $/h. The costs of exergy destruction (C_d), fuel (C_f) and product (C_p) were determined to be 55006.32 $/h, 66632.79 $/h, and 24664.78 $/h, respectively. The values of SI and EcoSI were determined as 1.254 and 1.211, respectively.

According to Fig. 12, the efficiency values are between 0.98324 and 0.99718. Therefore, the best design was determined as the design 1–1-5–1–1 with an efficiency score of 0.99718. In this design, $T_{1=}$ 133.5 °C, $T_{4=}$ 110 °C, $T_{37} = 111.99$ °C, $T_{41} = 95$ °C, $P_{41} = 1800$ kPa, $J = 1000$ A/m^2, $W_{PEMEL}/W_{ORC} = 10$ %. For this design, the energy and exergy efficiencies of the ORC were determined as 8.52 % and 20.48 %, respectively. The power generation rate was determined as 14.077 MW, whereas the net power generation was determined as 12.113 MW. The energy and exergy efficiencies of the PEMEL were determined as 50.38 % and 48.68 %, respectively. The hydrogen generation rate was determined as 0.005524 kg/s. The energy and exergy efficiencies of the overall system were determined as 8.05 % and 19.32 %, respectively. The investment cost (Z_k) was determined as 330.13 $/h. The costs of exergy destruction (C_d), fuel (C_f) and product (C_p) were determined to be 35518.44 $/h, 44680.63 $/h, and 23516.88 $/h, respectively. The values of SI and EcoSI were determined as 1.240 and 1.258, respectively.

According to Fig. 13, the efficiency values are between 0.98329 and 0.99713. Therefore, the best design was determined as the design 1–2-7–1-1 with an efficiency score of 0.99713. In this design, the optimization variables were determined as $T_{1=}$ 133.5 °C, $T_{4=}$ 110 °C, $T_{37} = 111.99$ °C, $T_{41} = 100$ °C, $P_{41} = 1950$ kPa, $J = 1000$ A/m^2, $W_{PEMEL}/W_{ORC} = 10$ %. For this design, the energy and exergy efficiencies of the ORC were determined as 8.78 % and 21.11 %, respectively. The power generation rate was determined as 14.077 MW, whereas the net power generation was determined as 12.113 MW. The energy and exergy efficiencies of the PEMEL were determined as 50.47 % and 48.76 %, respectively. The hydrogen generation rate was determined as 0.0057003 kg/s. The power generation rate was determined as 14.077 MW, whereas the net power generation was determined as 12.113 MW. The energy and exergy efficiencies of the overall system were determined as 8.30 % and 19.92 %, respectively. The investment cost (Z_k) was determined as 332.57 $/h. The costs of exergy destruction (C_d), fuel (C_f) and product (C_p) were determined at 38312.99 $/h, 48272.40 $/h, and 24240.05 $/h, respectively. The values of SI and EcoSI were determined as 1.249 and 1.260, respectively. The thermodynamic and economic properties of the optimal design (according to the design points given in Fig. 1) are given in Table 12. The energy, exergy and exergoeconomic analysis results are given in Table 13.

The comparative evaluation of the system is given in Table 14. The present system was compared to the systems given by Ref. [17] and Ref. [19].

According to Table 14, the designs conform with each other. The differences are sourced from the assumptions such as pump, turbine and heat exchanger efficiencies and the differences in the designs, such as the liquefying system and size of the subsystems.

The EATWOS results show the efficiency of the performance of designed systems based on the selected output criteria. Therefore, the higher EATWOS outputs indicate the better performance. According to the results, the increase in the weight of PEMEL in the systems decreases the efficiency score for all output criteria since the exergy efficiency of the system decreases. The SI-based outputs offer higher turbine inlet temperature and pressure since they enable more power generation with higher efficiency. EcoSI-based outputs offer lower turbine inlet temperature and pressure since they enable better economic outputs. However, the economic aspects become prominent when the investment is in question. The investors care about the economic issues as well as the performance of the systems. Since both the exergetic and economics are important for the designing stage, it would be better to evaluate the SI-based and EcoSI-based results together. So, the EATWOS outputs based on the combined effects give the more sensitive results for the designing stage.

4. Conclusion

This study investigates the optimum solution of the hybrid system, including power and hydrogen generation. The ORC and PEMEL are considered for this aim. R600a is used in ORC, whereas Nafion electrolyte and *Pt* electrodes are considered in PEMEL. The optimal system was determined by EATWOS multi-criteria decision-making analysis. For this purpose, a new decision-maker index was derived named EcoSI, including the exergoeconomic and sustainable index parameters. The hybrid system was designed to measure the performance of this new

system. According to the analyses, it was determined that EcoSI is a powerful decision maker compared to SI as well as exergy efficiency. The optimization shows that the integration of PEMEL decreases the hybrid system efficiency since it decreases with the increase of the power feeding rate. The PEMEL is efficient for the lower current density. According to the results of the increasing capacity of PEMEL, its integration into the ORC system decreases the sustainability of the geothermal energy sources. The most efficient case was obtained as the Design 1–2-7–1-1 with a turbine inlet temperature of 100 °C and inlet pressure of 1950 kPa. In this design, the optimal current density was determined as the minimum chosen value with 1000 A/m^2. The power supply rate was determined as the minimum chosen value with 10 %. The temperature difference between the production and re-injection wells was determined as 21.51 °C according to the optimal design. For this design, the energy and exergy efficiencies of the ORC were determined as 8.78 % and 21.11 %, respectively. The energy and exergy efficiencies of the PEMEL were determined as 50.47 % and 48.76 %, respectively. The energy and exergy efficiencies of the overall system were determined as 8.30 % and 19.92 %, respectively. The hydrogen generation rate was determined as 0.0057003 kg/s. The power generation rate was determined as 14.077 MW, whereas the net power generation was determined as 12.113 MW. The energy and exergy efficiencies of the overall system were determined as 8.30 % and 19.92 %, respectively. The investment cost (Z_k) was determined as 332.57 $/h. The costs of exergy destruction (C_d), fuel (C_F) and product (C_P) were determined to be 38312.99 $/h, 48272.40 $/h, and 24240.05 $/h, respectively. The values of SI and EcoSI were determined as 1.249 and 1.260, respectively.

The expanded poly-generation systems with the potential use of the handled geothermal resources can conduct more efficient systems as the future prospects. Also, different methods, such as genetic algorithms, Gray Wolf, and artificial neural networks with and without fuzzy points, can be performed to generate optimal designs for future research. Moreover, the new indexes can introduce environmental issues to EcoSI.

CRediT authorship contribution statement

Oguz Arslan: Writing – review & editing, Writing – original draft, Validation, Supervision, Methodology, Investigation, Formal analysis, Data curation, Conceptualization. **Asli Ergenekon Arslan:** Writing – original draft, Validation, Methodology, Investigation, Data curation.

Declaration of Competing Interest

The authors declare that they have no known competing financial interests or personal relationships that could have appeared to influence the work reported in this paper.

Data availability

No data was used for the research described in the article.

References

[1] A. von Jouanne and T. K. A. Brekken, “Ocean and Geothermal Energy Systems,” In: *Proceedings of the IEEE*, vol. 105, no. 11, pp. 2147-2165, Nov. 2017, doi: 10.1109/JPROC.2017.2699558.

[2] Arslan O, Yetik O. ANN based optimization of supercritical ORC-Binary geothermal power plant: Simav case study. Appl Therm Eng 2011;31(17–18):3922–8.

[3] Chitgar N, Hemmati A, Sadrzadeh M. A comparative performance analysis, working fluid selection, and machine learning optimization of ORC systems driven by geothermal energy. Energ Conver Manage 2023;286:117072.

[4] Altun AF, Kilic M. Thermodynamic performance evaluation of a geothermal ORC power plant. R*enewable Energy* 2020;148:261–74.

[5] Ozcan Z, Ekici O. A novel working fluid selection and waste heat recovery by an exergoeconomic approach for a geothermally sourced ORC system. Geothermics 2021;95:102151.

[6] Liu X, Wei M, Yang L, Wang X. Thermo-economic analysis and optimization selection of ORC system configurations for low temperature binary-cycle geothermal plant. Appl Therm Eng 2017;125:153–64.

[7] Huang W, Wang J, Lu Z, Wang S. Exergoeconomic and exergoenvironmental analysis of a combined heating and power system driven by geothermal source. Energ Conver Manage 2020;211:112765.

[8] Ren C, Wang J, Chen H, Liu X, An M. Thermodynamic analysis and comparative investigation of a new combined heating and power system driving by medium-and-high temperature geothermal water. Energ Conver Manage 2021;233:113914.

[9] Wang S, Liu C, Tang J, Xiao T, Huo E, Guan Z. Multi-mode and exergoeconomic analysis of a novel combined cooling, heating, and power system applied in the geothermal field. Energ Conver Manage 2023;276:116565.

[10] Caliskan H, Açıkkalp E, Takleh HR, Zare V. Advanced, extended and combined extended-advanced exergy analyses of a novel geothermal powered combined cooling, heating and power (CCHP) system. Renew Energy 2023;206:125–34.

[11] Ghorbani S, Deymi-Dashtebayaz M, Dadpour D, Delpisheh M. Parametric study and optimization of a novel geothermal-driven combined cooling, heating, and power (CCHP) system. Energy 2023;vol. 263(part F):126143.

[12] Ansarinasab H, Hajabdollahi H. Multi-objective optimization of a geothermal-based multigeneration system for heating, power and purified water production purpose using evolutionary algorithm. Energ Conver Manage 2020;223:113476.

[13] Ghiasirad H, Asgari N, Saray RK, Mirmasoumi S. Thermoeconomic assessment of a geothermal based combined cooling, heating, and power system, integrated with a humidification-dehumidification desalination unit and an absorption heat transformer. Energ Conver Manage 2021;235:113969.

[14] Mahmoud M, Ramadan M, Naher S, Pullen K, Abdelkareem MA, Olabi AG. A review of geothermal energy-driven hydrogen production systems. Thermal Science and Engineering Progress 2021;22:100854.

[15] Karayel GK, Javani N, Dincer I. Effective use of geothermal energy for hydrogen production: A comprehensive application. Energy 2022;249:123597.

[16] Cao Y, Haghghi MA, Shamsaiee M, Athari H, Ghaemi M, Rosen MA. Evaluation and optimization of a novel geothermal-driven hydrogen production system using an electrolyser fed by a two-stage organic Rankine cycle with different working fluids. J Storage Mater 2020;32:101766.

[17] Ghaebi H, Farhang B, Parikhani T, Rostamzadeh H. Energy, exergy and exergoeconomic analysis of a cogeneration system for power and hydrogen production purpose based on TRR method and using low grade geothermal source. Geothermics 2018;71:132–45.

[18] Yilmaz C. Life cycle cost assessment of a geothermal power assisted hydrogen energy system. Geothermics 2020;83:101737.

[19] Yilmaz C. Thermoeconomic modeling and optimization of a hydrogen production system using geothermal energy. Geothermics 2017;65:32–43.

[20] Mofrad KG, Zandi S, Salehi G. Exergoeconomic and exergoenvironmental assessment of a geothermal-driven cogeneration system utilizing dual-pressure organic Rankine cycle and zeotropic mixtures. Energy Rep 2023;9:5206–23.

[21] Baltacıoğlu MK, Yağlı H, Baydar C, Erdoğan Y. An alternative pathway from hot dry rock to green hydrogen by organic Rankine cycle applications. Int J Hydrogen Energy 2023;48(6):22855–64.

[22] Kianfard H, Khalilarya S, Jafarmadar S. Exergy and exergoeconomic evaluation of hydrogen and distilled water production via combination of PEM electrolyzer, RO desalination unit and geothermal driven dual fluid ORC. Energ Conver Manage 2018;177:339–49.

[23] Yuksel YE, Ozturk M, Dincer I. Thermodynamic analysis and assessment of a novel integrated geothermal energy-based system for hydrogen production and storage. Int J Hydrogen Energy 2018;43(9):4233–43.

[24] Ratlamwala TAH, Dincer I. Comparative efficiency assessment of novel multi-flash integrated geothermal systems for power and hydrogen production. Appl Therm Eng 2012;48:359–66.

[25] Yuksel YE, Ozturk M, Dincer I. Energetic and exergetic performance evaluations of a geothermal power plant based integrated system for hydrogen production. Int J Hydrogen Energy 2018;43(1):78–90.

[26] Yilmaz C, Kanoglu M. Thermodynamic evaluation of geothermal energy powered hydrogen production by PEM water electrolysis. Energy 2014;69:592–602.

[27] Han J, Wang X, Xu J, Yi N, Talesh SSA. Thermodynamic analysis and optimization of an innovative geothermal-based organic Rankine cycle using zeotropic mixtures for power and hydrogen production. Int J Hydrogen Energy 2020;45(15):8282–99.

[28] Cao Y, Mihardjo LWW, Farhang B, Ghaebi H, Parikhani T. Development, assessment and comparison of three high-temperature geothermal-driven configurations for power and hydrogen generation: Energy, exergy thermoeconomic and optimization. Int J Hydrogen Energy 2020;45(58):34163–84.

[29] Hasani MR, Nedaei N, Assareh E, Alirahmi SM. Thermo-economic appraisal and operating fluid selection of geothermal-driven ORC configurations integrated with PEM electrolyzer. Energy 2023;vol. 262(part B):125550.

[30] Alirahmi SM, Assareh E, Pourghassab NN, Delpisheh M, Barelli L, Baldinelli A. Green hydrogen & electricity production via geothermal-driven multi-generation system: Thermodynamic modeling and optimization. Fuel 2022;308:122049.

[31] Haghghi MA, Mohammadi Z, Delpisheh M, Nadimi E, Athari H. Multi-variable study/optimization of a novel geothermal-driven poly-generation system: Application of a soft-computing intelligent procedure and MOGWO. Process Saf Environ Prot 2023;171:507–31.

[32] J. Li, M. Zoghi, L. Zhao, “Thermo-economic assessment and optimization of a geothermal-driven tri-generation system for power, cooling, and hydrogen production,” *Energy*, vol. 244, part B, 123151, Apr. 2022.

[33] Li K, Ding YZ, Ai C, Sun H, Xu YP, Nedaei N. Multi-objective optimization and multi-aspect analysis of an innovative geothermal-based multi-generation energy

system for power, cooling, hydrogen, and freshwater production. Energy 2022;245:123198.
[34] Hekmatshoar M, Deymi-Dashtebayaz M, Gholizadeh M, Dadpour D, Delpisheh M. Thermoeconomic analysis and optimization of a geothermal-driven multi-generation system producing power, freshwater, and hydrogen. Energy 2022;247:123434.
[35] Arslan O, Arslan AE, Kurtbas I. Exergoeconomic and exergoenvironmental based multi-criteria optimization of a new geothermal district heating system integrated with thermal energy storage driven heat pump. Journal of Building Engineering 2023;73:106733.
[36] Sinha AA, Choudhary T, Ansari MZ. Sanjay, "Estimation of exergy-based sustainability index and performance evaluation of a novel intercooled hybrid gas turbine system". Int J Hydrogen Energy 2023;48:8629–44.
[37] Kaltakkıran G, Akolaş Hİ, Bakirci K. Evaluation of energy-exergy performance and sustainability index of a DI engine integrated with designed electromechanical EGR cooling system. Energ Conver Manage 2023;290:117229.
[38] Erol D, Yeşilyurt MK, Yaman H, Doğan B. Evaluation of the use of diesel-biodiesel-hexanol fuel blends in diesel engines with exergy analysis and sustainability index. Fuel 2023;337:126892.
[39] Arslan O, Kose R. Exergoeconomic optimization of integrated geothermal system in Simav, Kutahya. Energ Conver Manage 2010;51(4):663–76.
[40] Re-injection drilling operation of Simav Municipality. Available from: https://www.simav.bel.tr/proje/reenjeksiyon-sondaj-calismasi.
[41] Arslan O, Arslan AE, Boukelia TE. Modelling and optimization of domestic thermal energy storage based heat pump system for geothermal district heating. Energ Buildings 2023;282:112792.
[42] Arslan O, Ozgur MA, Kose R. Electricity generation ability of the Simav geothermal field: a techno-economic approach. Energy Sources Part A 2012;34:1130–44.
[43] Boukelia TE, Arslan O, Bouraoui A. Thermodynamic performance assessment of a new solar tower-geothermal combined power plant compared to the conventional solar tower power plant. Energy 2021;232:121109.
[44] Genceli OF. Heat Exchangers. Istanbul: Birsen Publishing; 1999.
[45] Ni M, Leung MKH, Leung DYC. Energy and exergy analysis of hydrogen production by a proton exchange membrane (PEM) electrolyzer plant. Energ Conver Manage 2008;49(10):2748–56.
[46] Thampan T, Malhotra S, Zhang JX, Datta R. PEM fuel cell as a membrane reactor. Catal Today 2001;67(1):15–32.
[47] Gurau V, Barbir F, Liu HT. An analytical solution of a half-cell model for PEM fuel cells. Journal of Electrochemical Society 2000;147(7):2468–77.
[48] Chan SH, Xia ZT. Polarization effects in electrolyte/electrode-supported solid oxide fuel cells. J Appl Electrochem 2002;32(3):339–47.
[49] M. Ni, M.K.H. Leung, D.Y.C Leung, "Electrochemistry modelling of proton Exchange membrane (PEM) water electrolysis for hydrogen production" presented at the Proceedings of the 16th World Hydrogen Energy Conference, Lyon, France, Jun. 13-16, 2006. Available from: https://www.cder.dz/A2H2/Medias/Download/ Proc%20PDF/posters/%5bGII%5d%20Production%20from%20electrolysis%20&%20thermochemical%20cycles/018.pdf.
[50] Markovic NM, Grgur BN, Ross PN. Temperature-dependent hydrogen electrochemistry on platinum low-index single-crystal surfaces in acid solutions. Journal of the Physical Chemistry B 1997;101:5405–13.
[51] Beattie PD, Basura VI, Holdcroft S. Temperature and pressure dependence of O2 reduction at Pt/Nafion 117 and Pt/BAM 407 interfaces. J Electroanal Chem 1999;468(2):180–92.
[52] Arslan O. Performance analysis of a novel heat recovery system with hydrogen production designed for the improvement of boiler effectiveness. Int J Hydrogen Energy 2021;46(10):7558–72.
[53] Arslan O, Acikkalp E, Genc G. A multi-generation system for hydrogen production through the high-temperature solid oxide electrolyzer integrated to 150 MW coal-fired steam boiler. Fuel 2022;315:123201.
[54] Bejan A, Tsatsaronis G, Moran MJ. Thermal Design and Optimization. New York: John Wiley and Sons; 1996.
[55] Anonymous. (2022, Dec.). Inflation report. Central Bank of Republic of Turkey. Available from: https://www.tcmb.gov.tr/wps/wcm/connect/EN/TCMB+EN/Main+Menu/Core+Functions/Monetary+Policy/Rediscount+and+Advance+Interest+Rates.
[56] Yang Liu, Jitian Han, Huailiang You, "Exergoeconomic analysis and multi-objective optimization of a CCHP system based on LNG cold energy utilization and flue gas waste heat recovery with CO2 capture, "*Energy*, vol. 190, 116201, Jan. 2020.
[57] C. Maxwel. (2023, Mar.). Cost indices. Towering skills. Available from: https://www.toweringskills.com/financial-analysis/cost-indices/#cepci-2001-to-present.
[58] Malik MZ, Musharavati F, Khanmohammadi S, Pakseresht AH, Khanmohammadi S, Nguyen DD. Design and comparative exergy and exergo-economic analyses of a novel integrated Kalina cycle improved with fuel cell and thermoelectric module. Energ Conver Manage 2020;220:113081.
[59] Aminyavari M, Najafi B, Shirazi A, Rinaldi F. Exergetic, economic and environmental (3E) analyses, and multi-objective optimization of a CO2/NH3 cascade refrigeration system. Appl Therm Eng 2014;65(1–2):42–50.
[60] Mosaffa AH, Hasani Mokarram N, Garousi Farshi L. "Thermo-economic analysis of combined different ORCs geothermal power plants and LNG cold energy". Geothermics 2017;65:113–25.
[61] Amir Reza Razmi. Seyed Mojtaba Alirahmi, Mohammad Hossein Nabat, Ehsanolah Assareh, Mahdi Shahbakhti, "A green hydrogen energy storage concept based on parabolic trough collector and proton exchange membrane electrolyzer/fuel cell: Thermodynamic and exergoeconomic analyses with multi-objective optimization". Int J Hydrogen Energy 2022;47(62):26468–89.
[62] Luyben WL. Capital cost of compressors for conceptual design. Chem Eng Process - Process Intesif 2018;126:206–9.
[63] U. Senturk. (2017, Sep.). Interview on the jeothermal plant analysis. JESDER. Available from: https://yesilhaber.net/jeotermal-enerji-yatirim-maliyeti-nukleer le-yarisiyor/.
[64] Lu F, Zhu Y, Pan M, Li C, Yin J, Huang F. Thermodynamic, economic, and environmental analysis of new combined power and space cooling system for waste heat recovery in waste-to-energy plant. Energ Conver Manage 2020;226:113511.
[65] Arslan O, Arslan AE. Performance evaluation and multi-criteria decision analysis of thermal energy storage integrated geothermal district heating system. Process Saf Environ Prot 2022;167:21–33.
[66] M.L. Peters, S. Zelewski, "Efficiency analysis under consideration of satisficing levels for output quantities," In: *Proc. of the 17th Annual Conference of the Production and Operations Management Society*, Boston, USA, 2006, pp. 2-18.
[67] REFPROP. *Reference Fluid thermodynamics and transport properties, NIST reference database*, Version 9.0. NIST, USA: National Institute of Standards and Technology; 2010.
[68] Ioroi T, Yasuda K, Siroma Z, Fujiwara N, Miyazaki Y. Thin film electrocatalyst layer for utilized regenerative polymer electrolyte fuel cells. J Power Sources 2002;112(2):583–7.